

Probing into Decay Products at Finite Distance in Muon Decay

Kenzo Ishikawa, Tasuku Nozaki, Masashi Sentoku, and Yutaka Tobita

*Department of Physics, Faculty of Science,
Hokkaido University, Sapporo 060-0810, Japan*

(Dated: December 6, 2024)

Abstract

The probabilities of the events that the neutrino or electron from muon are detected in the time interval $T \leq \tau_\mu$ reveal the particle and wave characteristics and are expressed as $T\Gamma^0 + P^{(d)}$, where the former has been known long time but the latter is found recently. Γ^0 is computed with Fermi's golden rule and has universal properties irrespective of the initial wave function. $P^{(d)}$ is computed differently including the overlap of the initial and final wave functions, and becomes significant for light particles. Having the origin in wave natures, $P^{(d)}$ satisfies different properties from Γ^0 , and affects strongly to physical quantities of the decay, in the distance $L \leq L_0$, and $L \leq c\tau_\mu$, where $L_0 = m_\nu^2/(2E_\nu)$ for the neutrino and τ_μ is the life-time of muon. Including $P^{(d)}$ of three neutrinos, all neutrino experiments made to confirm LSND data can be explained consistently.

CONTENTS

I. Introduction	3
II. S-matrix at a finite time-interval, $S[T]$, for muon decays	8
A. Properties of wave packets	8
B. Different matter effects in μ^+ and μ^-	10
III. The electron neutrino	11
A. Asymptotic spectrum and rate	11
B. Position dependent amplitude from $S[T]$	12
C. Probability	13
D. Normal term	14
E. Finite-size corrections: spectral representation	14
F. Energy spectrum	19
1. Diffraction component	19
2. Normal component	19
G. Mean life-time at a finite distance	21
H. Size of neutrino wave packet	21
I. Mixing effect on diffraction term	21
IV. Implications to neutrino experiments	24
A. ν_e and $\bar{\nu}_\mu$ in μ^+ decay	25
1. μ^+ decay at rest (μ^+ DAR)	25
2. μ^+ decay in flight (μ^+ DIF)	26
3. Excess of electron neutrino in accelerator experiments	28
B. Neutrino flavor changes through diffraction in μ^+ decay	29
1. LSND and KARMEN (μ^+ DAR)	31
2. Future experiments of μ^+ DAR and μ^+ DIF	34
V. The electron spectrum	38
A. Asymptotic value	39
B. Probability	39

VI. Summary	42
Acknowledgments	44
A. Life-time effect on normal term	44
B. Light-cone singularity	45
1. Vacuum expectation value	46
a. Real mass	46
b. Imaginary mass	47
2. Single particle expectation value	47
a. High spin component	48
3. Many-particle expectation value	48
a. Two-particle: neutrino and electron	49
b. Two-particle: two neutrinos	49
C. Universal function $\tilde{g}(\omega, T; \tau_\mu)$	50
1. General form of $\tilde{g}(\omega_\nu, T; \tau_\mu)$	51
a. Without mixing	51
b. Mixing case	52
2. Large life-time and T	54
a. Asymptotic behavior	54
3. Large mass	54
4. Angle dependence of overlapping region T	55
5. σ_μ dependence	56
a. DAR	56
b. DIF	56
References	56

I. INTRODUCTION

The probabilities of particle's two body decays of life-time τ computed with Fermi's golden rule get large corrections at $T \leq \tau$ for light particles due to quantum interference

[1, 2], where T is time interval between in and out states. Transition probabilities measured at the finite distance cT deviate from those at asymptotic region $T \rightarrow \infty$, because the overlap of wave function of daughters with that of parent which disappears at $T \rightarrow \infty$ is finite at a finite T . An S-matrix, $S[\infty]$, satisfies boundary conditions of asymptotic region $T \rightarrow \infty$ [3] and is not applicable if T is finite. Another S-matrix that satisfies the boundary conditions at finite T , $S[T]$, was formulated and applied to compute the probability of events that the decay product is detected at T [4]. The deviations of the value at T from that at $T \rightarrow \infty$ become significant when their overlap becomes substantial, because an interaction Hamiltonian has finite-expectation value, and kinetic energy of daughter deviates from that of parent. Figure 1 shows the difference between $T \rightarrow \infty$ and $T < \tau$ using two body decay. The amplitude expressed with $S[T]$ in the pion decay [2] leads the probability in the form,

$$P = T\Gamma^0 + P^{(d)}, \quad (1)$$

where Γ^0 agrees with that computed with Fermi's golden rule using $S[\infty]$. $P^{(d)}$ does not satisfy the conservation law of kinetic energy which holds in Γ^0 , and the energy spectrum from $P^{(d)}$ is continuous whereas that from Γ^0 is discrete in two body decay. New physical quantities are derived from $P^{(d)}$ and are in accord with experiments.

The analyses are extended to muon decay in the present paper. The muon decays to the electron, electron neutrino, and muon neutrino, and has longer life time than pion. Accordingly, there are several new observables, which can be measured in experiments and may supply important informations. The neutrino and electron are studied at $T \leq \tau_\mu$ with $S[T]$, where τ_μ is the life-time of muon. The probability is expressed in the same expression as the two body decay, Eq. (1), where Γ^0 agrees with that computed with Fermi's golden rule using $S[\infty]$ and $P^{(d)}$ is computed with $S[T]$. Energy spectra of a neutrino and electron and decay rates in

$$\mu^- \rightarrow e^- + \bar{\nu}_e + \nu_\mu, \quad (2)$$

$$\mu^+ \rightarrow e^+ + \nu_e + \bar{\nu}_\mu, \quad (3)$$

at $T \leq \tau_\mu$ become different from those of the asymptotic region due to $P^{(d)}$. The spectra are continuous in both cases, and the deviation is less prominent compared to two body decays but is sizable. Thus, decay products retain wave natures in the overlapping region. A space-time region for out-going fields to show the wave nature is called wave zone, and the other

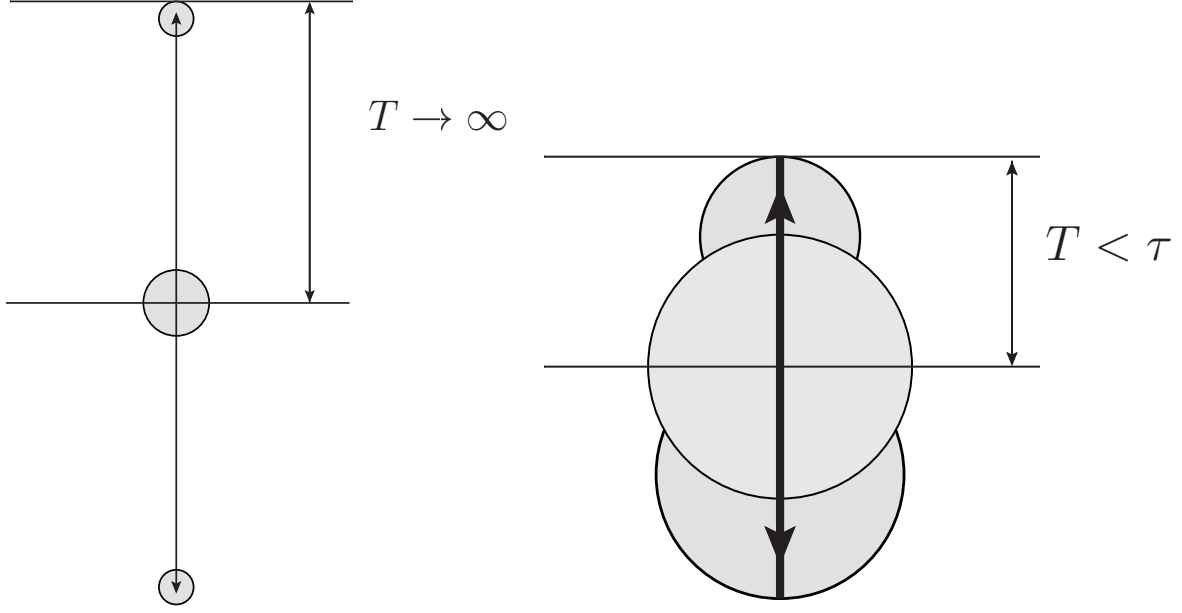


FIG. 1. Two body decays of a particle of life time τ at $T \rightarrow \infty$ (left) and $T < \tau$ (right). At $T \rightarrow \infty$ the initial state does not overlap with the final state but at $T < \tau$, the initial state overlaps with the final state. Because of this overlapping region, kinetic energy does not conserve at $T < \tau$.

is called the particle zone. The boundary between those two zones are given later. Neutrino has extremely small mass and propagates with almost the speed of light. Since the group of neutrino waves have almost same phase and group velocity, their relative phases are kept constant in a certain period. Furthermore, it interacts extremely weakly with matter, and is not disturbed by environment. Thus observations of the quantum interference of neutrino formed in large wave zone become possible even at a macroscopic distance. They might be achieved with neutrino experiments at near-detectors, which have detected a large number of neutrino events.

Muon decay is governed by the charged current weak interaction

$$H_{\text{int}} = \frac{G_F}{\sqrt{2}} \int d\vec{x} (\bar{\mu}(x) (1 - \gamma_5) \gamma_\mu \nu_\mu(x)) (\bar{e}(x) (1 - \gamma_5) \gamma^\mu \nu_e(x))^\dagger, \quad (4)$$

and has a long life-time, hence the parent coexists with daughters for a long period. This state is a superposition of both states, and follows the Schrödinger equation,

$$i\hbar \frac{\partial}{\partial t} |\Psi(t)\rangle = H |\Psi(t)\rangle = (H_0 + H_{\text{int}}) |\Psi(t)\rangle, \quad (5)$$

$$H_0 = \int d\vec{x} \left(\bar{l}(x) \left(\vec{\alpha} \cdot \vec{\nabla} + \beta m_l \right) l(x) + \bar{\nu}(x) \left(\vec{\alpha} \cdot \vec{\nabla} + \beta m_\nu \right) \nu(x) \right),$$

where G_F is the Fermi coupling constant. A fermion field is expanded with annihilation and creation operators as

$$\psi(x) = \sum_s \int \frac{d\vec{p}}{(2\pi)^{\frac{3}{2}}} \left(\frac{m}{E(\vec{p})} \right)^{\frac{1}{2}} \left\{ u(\vec{p}, s) b(\vec{p}, s) e^{-ip \cdot x} + v(\vec{p}, s) b^\dagger(\vec{p}, s) e^{ip \cdot x} \right\}, \quad (6)$$

$$\{b(\vec{p}_1, s_1), b^\dagger(\vec{p}_2, s_2)\} = \delta(\vec{p}_1 - \vec{p}_2) \delta_{s_1, s_2}.$$

One muon state of the momentum eigenstate at $t = 0$,

$$|\Psi(0)\rangle = |\mu, \vec{p}_\mu\rangle, \quad \langle\mu, \vec{p}_1|\mu, \vec{p}_2\rangle = \delta(\vec{p}_1 - \vec{p}_2) \quad (7)$$

becomes a sum of the muon and decay products at a later time t ,

$$|\Psi(t), \vec{p}\rangle = a_0(t) |\mu, \vec{p}_\mu\rangle + \int d\vec{p}_l d\vec{p}_{\nu_e} d\vec{p}_{\nu_\mu} a_1(t, \vec{p}_e, \vec{p}_{\nu_e}, \vec{p}_{\nu_\mu}) |e, \vec{p}_e; \nu_e, \vec{p}_{\nu_e}; \nu_\mu, \vec{p}_{\nu_\mu}\rangle, \quad (8)$$

where the coefficients are

$$a_0(t) = e^{-i\frac{E_\mu}{\hbar}t - \frac{t}{\tau_\mu}}, \quad (9)$$

$$a_1(t, \vec{p}_e, \vec{p}_{\nu_e}, \vec{p}_{\nu_\mu}) = e^{-i\frac{E_\mu}{\hbar}t} \frac{e^{-i\frac{\omega}{\hbar}t} - e^{-\frac{t}{\tau_\mu}}}{\omega + i\frac{\hbar}{\tau_\mu}} \langle e, \vec{p}_e; \nu_e, \vec{p}_{\nu_e}; \nu_\mu, \vec{p}_{\nu_\mu} | H_{\text{int}} | \mu, \vec{p}_\mu \rangle, \quad (10)$$

in the lowest order of G_F with an exception on the life-time, which is given by the total rate proportional to G_F^2 , where $\omega = E_e + E_{\nu_e} + E_{\nu_\mu} - E_\mu$. H_{int} causes the transition and expectation values are given as,

$$\langle\mu, \vec{p}_\mu | H_{\text{int}} | \mu, \vec{p}_\mu \rangle = 0, \quad (11)$$

$$\langle e, \vec{p}_e; \nu_e, \vec{p}_{\nu_e}; \nu_\mu, \vec{p}_{\nu_\mu} | H_{\text{int}} | e, \vec{p}_e; \nu_e, \vec{p}_{\nu_e}; \nu_\mu, \vec{p}_{\nu_\mu} \rangle = 0, \quad (12)$$

$$\begin{aligned} & \langle e, \vec{p}_e; \nu_e, \vec{p}_{\nu_e}; \nu_\mu, \vec{p}_{\nu_\mu} | H_{\text{int}} | \mu, \vec{p}_\mu \rangle \\ &= N \frac{G_F}{\sqrt{2}} (2\pi)^3 \delta^{(3)}(\delta\vec{p}) \bar{\mu}(\vec{p}_\mu) (1 - \gamma_5) \gamma_\mu \nu_\mu(\vec{p}_{\nu_\mu}) (\bar{e}(\vec{p}_e) (1 - \gamma_5) \gamma^\mu \nu_\mu(\vec{p}_{\nu_e}))^*, \end{aligned} \quad (13)$$

where $\delta\vec{p} = \vec{p}_\mu - \vec{p}_e - \vec{p}_{\nu_e} - \vec{p}_{\nu_\mu}$ and explicit form of N is given in Sec. 2. Accordingly the expectation value of the interaction Hamiltonian becomes

$$\begin{aligned} \frac{\langle\Psi(t)|H_{\text{int}}|\Psi(t)\rangle}{\langle\Psi(t)|\Psi\rangle} &= 2\text{Re} [a^*(t)b(t, \vec{p}_e, \vec{p}_{\nu_e}, \vec{p}_{\nu_\mu}) \langle\mu, \vec{p}_\mu | H_{\text{int}} | e, \vec{p}_e; \nu_e, \vec{p}_{\nu_e}; \nu_\mu, \vec{p}_{\nu_\mu} \rangle] \\ &= 2\zeta(t, \tau_\mu) \left| \langle e, \vec{p}_e; \nu_e, \vec{p}_{\nu_e}; \nu_\mu, \vec{p}_{\nu_\mu} | H_{\text{int}} | \mu, \vec{p}_\mu \rangle \right|^2, \end{aligned} \quad (14)$$

$$\zeta = e^{-\frac{t}{\tau_\mu}} \frac{\omega \cos(\omega t/\hbar) - \omega e^{-\frac{t}{\tau_\mu}} - \frac{\hbar}{\tau_\mu} \sin(\omega t/\hbar)}{\omega^2 + \frac{\hbar^2}{\tau_\mu^2}}. \quad (15)$$

Consequently

$$\langle \Psi(t) | H_{\text{int}} | \Psi(t) \rangle = 0; \quad t = 0, \infty, \quad (16)$$

$$\langle \Psi(t) | H_{\text{int}} | \Psi(t) \rangle \neq 0; \quad 0 < t < \tau_\mu, \quad (17)$$

due to an overlap of wave functions between $|\mu\rangle$ and $|e, \nu_e, \nu_\mu\rangle$ in $0 < t < \tau_\mu$. Since

$$i\hbar \frac{d}{dt} \langle \Psi(t) | H | \Psi(t) \rangle = \langle \Psi(t) | [H, H] | \Psi(t) \rangle = 0, \quad (18)$$

the total energy is conserved but the expectation value of $i\hbar \frac{\partial}{\partial t} - E_\mu$ becomes

$$\langle \Psi(t) | i\hbar \frac{\partial}{\partial t} - E_\mu | \Psi(t) \rangle = \langle \Psi(t) | H_{\text{int}} | \Psi(t) \rangle \begin{cases} = 0; & t = 0, \infty, \\ \neq 0; & 0 < t < \tau_\mu. \end{cases} \quad (19)$$

Thus, the energy defined by the Einstein's relation from frequency is different from the initial energy, E_μ , and varies in time in $0 < t < \tau_\mu$. The expectation value of daughter's energy becomes non-uniform in time and deviates from E_μ . The deviation can be as large as of $O(1)$ in magnitude. The non-uniform behavior of the sum of waves of various wave lengths is generally called diffraction, and **the probability to detect the decay product reveals the diffraction that depends on a distance in this region**. Because the amplitude in the tree level is defined uniquely regardless of higher-order corrections, this position-dependent probability is a meaningful physical quantity.

$S[T]$ that satisfies the boundary condition at T is expressed with wave packets that are localized in space. $S[T]$ gives identical results as $S[\infty]$ in certain large T , and different ones in small T [1]. Furthermore, as was shown in Fig. 1 if the size of wave denoted as σ is small, the overlapping region becomes small and the diffractive effect also becomes small. So, the effect is sensitive to the boundary conditions including T and σ .

A characteristic minimum length in space of the former region is the coherence length L_c . L_c depends on dynamical properties and detection method, and was found to be

$$L_c = \frac{\hbar}{mc} \times \frac{E}{mc^2}, \quad (20)$$

where c , E , and m are the speed of light, the energy and mass of detected particle, respectively in two body decays [1]. The boundary between the wave zone and particle zone is determined with L_c . In the wave zone, the probability of the event to detect the particle shows diffraction and varies in the direction parallel to the momentum of detected particle.

The diffraction pattern that is sensitive to the absolute mass of detected particle appears in the distribution of events and plays an important role for a neutrino detection because L_c can be exceptionally large for neutrinos from Eq. (20). Since m is extremely small for neutrino and large for electron, the finite-size correction as diffraction is much large for the neutrino, if σ is the same. We find that the three body decay is the same.

One of neutrino's fundamental constants is its absolute mass. Mass squared differences are found from flavor oscillations [5],

$$\Delta m_{21}^2 = m_2^2 - m_1^2 = 7.58_{-0.26}^{+0.22} \times 10^{-5} \text{ eV}^2/c^4, \quad (21)$$

$$|\Delta m_{23}^2| = |m_2^2 - m_3^2| = 2.35_{-0.09}^{+0.12} \times 10^{-3} \text{ eV}^2/c^4, \quad (22)$$

where m_i , ($i = 1 - 3$) are mass values. Tritium beta decay has been used for determining the absolute value but the existing upper bound for the effective-electron-neutrino mass squared is of the order of $2 \text{ eV}^2/c^4$ [6]. From cosmology, the bounds for a sum of masses are $\sum_i m_i \leq 0.44 \text{ eV}/c^2$ [7, 8] and $\sum_i m_i \leq 0.23 \text{ eV}/c^2$ [9]. We will see that the small absolute mass is subject of observations.

The present paper is organized in the following manner. In section 2, some generalities on $S[T]$ of the muon decay process are given. In section 3, the electron neutrino is studied and its implications to the neutrino experiments in muon decays are presented in Section 4. Section 5 is devoted to the electron spectrum and its implications to the ground precision experiments. Summary is given in Section 6.

II. S-MATRIX AT A FINITE TIME-INTERVAL, $S[T]$, FOR MUON DECAYS

A. Properties of wave packets

$S[T]$ is described with wave functions of finite sizes, i.e., wave packets, which are localized in space around their centers [4, 10] in order to express the scattering process at T . The sizes of wave packets of the muon, electron, and neutrinos are evaluated from their physical reactions. The muon is studied first. Since the muon is produced by decay of pion from proton collision, the spatial size of proton is necessary to determine the size of the wave function of the muon. As was shown in Ref. [10], the size of the particle in matter is determined by its mean free path. For the charged particle, the size is determined by the

cross section of Coulomb scattering with atoms. The energy loss is also determined by the same cross section and is summarized in particle data summary [5]. From their energy loss rates for several metals such as Pb, Fe, and others, a mean free path of proton of 1 GeV/c was estimated as $L_{\text{proton}} = 50 - 100$ cm and at lower momentum of 2 MeV/c, $L_{\text{proton}} = 10$ cm.

The size of pion produced in high-energy proton collisions with target nucleus is computed using the above values of the proton and target size. In relativistic-energy region, particles have the speed of light and in the pion production process, the size of pion, δx_π , is connected with those of the proton δx_{proton} in the form, $\frac{\delta x_{\text{proton}}}{v_{\text{proton}}} = \frac{\delta x_\pi}{v_\pi}$, $\delta x_\pi = \frac{v_\pi}{v_{\text{proton}}} \delta x_{\text{proton}} \approx \delta x_{\text{proton}}$, where v_i is the speed of particle. Consequently pion's size of momentum 1 GeV/c or larger is given by $\delta x_\pi \approx 40 - 100$ cm. Since the muon is produced from pion decay, its size is determined by similar way. Muon's size is connected with the pion's size and their speeds, $\frac{\delta x_\pi}{v_\pi} = \frac{\delta x_\mu}{v_\mu}$, and is expressed in the form $\delta x_\mu = \frac{v_\mu}{v_\pi} \delta x_\pi$. For the relativistic particles, the speeds are almost the speed of light and their ratio is unity. So we have $\delta x_\mu = \delta x_\pi$. Hence, the size of the muon of the energy around 1 GeV/c is given as $\delta x_\mu \approx 40 - 100$ cm.

Next, the sizes of detected particles are studied. A neutrino rarely interacts with matter and the probability of the events that the neutrino is detected is determined by the probability amplitude of its reactions with a nucleus or atom in detector. They are described by wave functions of finite sizes, and the matrix element is written with these wave packets. Accordingly the size of the nucleus or electron determines the size of the wave function of the neutrino in the transition amplitude. This size is different from the neutrino's mean free path, off course. Nuclei have sizes of the order of 10^{-15} m and the electrons bounded in atom have sizes of the order of 10^{-10} m. The neutrino wave functions of these sizes are used for out-going neutrino states of the decay. The shape of the wave packet is known approximately. For the neutrino identified by incoherent scattering with a nucleus or electron, the nucleus or electron wave function determines the shape. Density of nucleus is constant in the bulk and decreases smoothly toward the edge and that of electron is almost the same. So we apply Gaussian wave packets for the neutrino and estimate the corrections perturbatively. We found that the corrections due to non-Gaussian form are almost negligible in the previous work [2], and that the long-range behavior of the position-dependent probability is independent from the shape of the wave packet and is universal. Hence, the Gaussian wave packets are applied throughout this paper.

B. Different matter effects in μ^+ and μ^-

μ^+ and μ^- decay in symmetric manner in vacuum with the mean life-time at rest

$$\tau_\mu = 2.2 \times 10^{-6} \text{ sec.} \quad (23)$$

They have opposite charge and interact with atoms differently, hence behave in asymmetric manner in matter. μ^- can form a bound state due to an attractive force of nucleus, which has a small wave function. Whereas μ^+ does not form bound state, and is expressed approximately by a plane wave or other large wave function. Consequently, the former wave functions have small sizes, and the latter have large sizes.

At high energy, the waves in scattering states lose energies by the interaction with atoms and stay in one state for finite periods. Their average lengths are determined by mean free paths,

$$l_\mu = \frac{1}{n\sigma_{\text{cross}}}, \quad (24)$$

where n and σ_{cross} is density of scatterers and cross section respectively. The transition rate and average life-time of the velocity v are

$$\Gamma = n\sigma_{\text{cross}}v = \frac{v}{l}, \quad (25)$$

$$\tau_{\text{int}} = \frac{1}{\Gamma}. \quad (26)$$

High energy μ^\pm in matter remain in one state for a time interval τ_{int} . At around 1 GeV/c, the mean free path is about 50 – 100 cm. At 0.1 GeV/c, the value is about 5 – 10 cm. They lose their energies and stop afterward.

For the stopped μ^+ , the wave functions in solids of periodic potential due to atoms are extended waves of continuous energies. They are plane waves of phase shifts, and are extended in space. Thus μ^+ at rest, $v = 0$, is described by the wave function of large size. The stopped μ^- can form bound states, and their wave functions are localized of discrete energies. Thus μ^- at rest are described by the wave function of small sizes. Consequently, the decay of μ^+ at rest (μ^+ DAR) is studied with the initial state of plane waves and the decay of μ^- at rest (μ^- DAR) is studied with the initial state of bound states. For both μ^\pm decays in flight (μ^\pm DIF), they are produced from decays of π^\pm and retain coherence of same size of π^\pm . So it is good approximations to treat μ^\pm as plane waves [2].

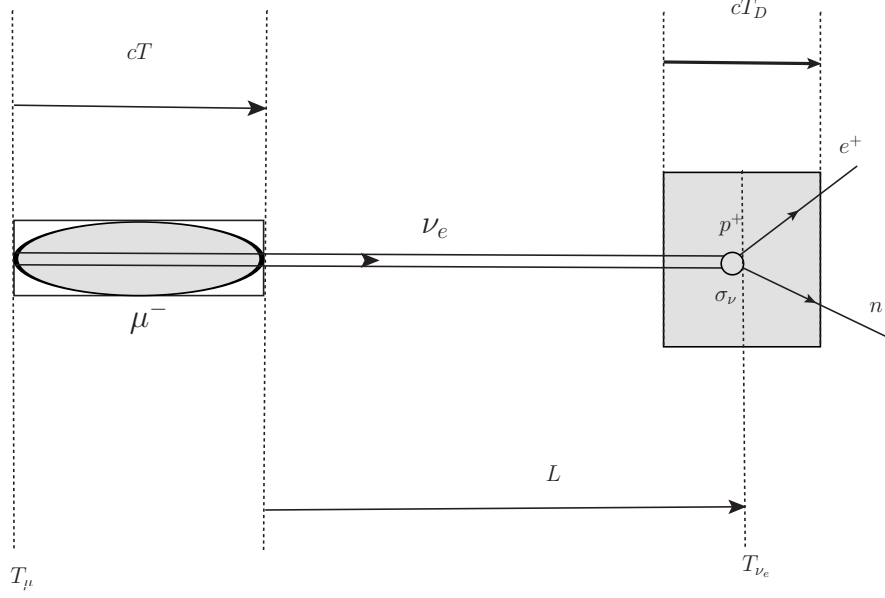


FIG. 2. The geometry of μ^- decay at rest is shown. In real experiments, a detector of cT_D m long is located away from decay region. However, in Sec. 3 we study a case where a detector is located in front of decay region, that is, $L = 0$ for simplicity.

III. THE ELECTRON NEUTRINO

The finite-size correction to the rate of the event that the electron neutrino is detected is studied in this section. The geometry of muon decay at rest is shown in Fig. 2. In this section, the length between decay region and detector denoted L is set to zero for simplicity.

A. Asymptotic spectrum and rate

The rate and spectrum of the electron neutrino at the asymptotic region, $T \rightarrow \infty$ are known as

$$\Gamma^0 = \frac{G_F^2 m_\mu^5}{192\pi^3}, \quad (27)$$

$$\frac{d\Gamma^0}{dE_{\nu_e}} = \frac{G_F^2}{2\pi^3} m_\mu^2 E_{\nu_e}^2 \left(1 - \frac{2E_{\nu_e}}{m_\mu}\right) \quad (28)$$

in the lowest order of G_F for the plane waves of the parent μ at rest and daughters. The electron mass and the radiative corrections were neglected in Eqs. (27) and (28).

B. Position dependent amplitude from $S[T]$

The position-dependent matrix element of $S[T]$ for the process to detect the neutrino by its reaction with a material in a detector is obtained hereafter. The size of neutrino wave function is denoted as σ_ν [12]. The case without mixing of neutrino is studied first for simplicity. The amplitude from an initial state $|\mu\rangle$ to a final state $|e, \nu_\mu, \nu_e\rangle$ is

$$\mathcal{M} = \int d^4x \langle e, \nu_\mu, \nu_e | H_{\text{int}} | \mu \rangle, \quad (29)$$

where particles and anti-particles are treated without distinction. e and ν_μ are expressed by plane waves and others are expressed by wave packets specified by central values of momenta, coordinates, and times,

$$|\mu\rangle = |\vec{p}_\mu, \vec{X}_\mu, T_\mu\rangle, \quad (30)$$

$$|e, \nu_\mu, \nu_e\rangle = |\vec{p}_e, \vec{p}_{\nu_\mu}, \vec{p}_{\nu_e}, \vec{X}_{\nu_e}, T_{\nu_e}\rangle. \quad (31)$$

Substituting weak Hamiltonian, we have

$$\mathcal{M} = \frac{G_F}{\sqrt{2}} \int d^4x \langle \vec{p}_{\nu_\mu} | J_\rho^{V-A}(x) | \vec{p}_\mu, \vec{X}_\mu, T_\mu \rangle \langle \vec{p}_e, \vec{p}_{\nu_e}, \vec{X}_{\nu_e}, T_{\nu_e} | J_{V-A}^\rho(x) | 0 \rangle, \quad (32)$$

where the matrix elements are expressed in the forms,

$$\langle \vec{p}_{\nu_\mu} | J_\rho^{V-A}(x) | \vec{p}_\mu, \vec{X}_\mu, T_\mu \rangle = N_\mu \varrho_\mu \varrho_{\nu_e} \int d\vec{k}_\mu e^{-\frac{\sigma_\mu}{2}(\vec{k}_\mu - \vec{p}_\mu)^2} e^{-i(\phi_\mu(x, \vec{k}_\mu) - \phi_{\nu_\mu}(x, \vec{p}_{\nu_\mu}))} (J_{\mu, \nu_\mu})_\rho, \quad (33)$$

$$\langle \vec{p}_e, \vec{p}_{\nu_e}, \vec{X}_{\nu_e}, T_{\nu_e} | J_{V-A}^\rho(x) | 0 \rangle = N_{\nu_e} \varrho_e \varrho_{\nu_e} \int d\vec{k}_{\nu_e} e^{-\frac{\sigma_{\nu_e}}{2}(\vec{k}_{\nu_e} - \vec{p}_{\nu_e})^2} e^{i\phi_e(x, \vec{p}_e) + i\phi_{\nu_e}(x, \vec{k}_{\nu_e})} (J_{e, \nu_e})^\rho, \quad (34)$$

$$(J_{\alpha, \beta})^\rho = \bar{u}(\vec{p}_\alpha) \gamma^\rho (1 - \gamma_5) u(\vec{k}_\beta). \quad (35)$$

In Eqs. (33) and (34),

$$N_\mu = \left(\frac{\sigma_\mu}{\pi} \right)^{\frac{3}{4}}, \quad N_{\nu_e} = \left(\frac{\sigma_{\nu_e}}{\pi} \right)^{\frac{3}{4}}, \quad \varrho_\alpha = \left(\frac{m_\alpha}{(2\pi)^3 E_\alpha} \right)^{\frac{1}{2}}, \quad (36)$$

and the phase factors $\phi_\alpha(x)$ are given in the form

$$\phi_\alpha(x, \vec{k}_\alpha) = E(\vec{k}_\alpha)(t - T_\alpha) - \vec{k}_\alpha \cdot (\vec{x} - \vec{X}_\alpha), \quad (\alpha = \mu, \nu_e), \quad (37)$$

$$\phi_\beta(x, \vec{p}_\beta) = E(\vec{p}_\beta)t - \vec{p}_\beta \cdot \vec{x}, \quad (\beta = e, \nu_\mu). \quad (38)$$

The spinor is normalized as,

$$\sum_s (u^{(s)}(\vec{p}) \bar{u}^{(s)}(\vec{p})) = \frac{\gamma \cdot p + m}{2m}. \quad (39)$$

The integral of the product of Gaussian wave packet and a slowly varying function $f(\vec{k})$ is computed approximately in the form,

$$\int d\vec{k} e^{-\frac{\sigma}{2}(\vec{k}-\vec{p})^2 - i\phi(x, \vec{k})} f(\vec{k}) \approx \left(\frac{2\pi}{\sigma}\right)^{\frac{3}{2}} w(x, X; \sigma) e^{-i\phi(x, \vec{p})} f(\vec{p})(1 + \delta_f), \quad (40)$$

$$w(x, X; \sigma) = e^{-\frac{1}{2\sigma}(\vec{x}-\vec{X}-\vec{v}(t-T))^2}, \quad \vec{v} = \frac{\vec{p}}{E(\vec{p})}, \quad (41)$$

at small $|t - T|$ region where the correction δ_f is negligible.

Finally, the amplitude is written in the form

$$\mathcal{M} = \frac{G_F}{\sqrt{2}} \tilde{N} f I(\delta p), \quad \delta p = p_\mu - p_e - p_{\nu_\mu} - p_{\nu_e}, \quad (42)$$

$$I(\delta p) = \int_{T_\mu}^{T_{\nu_e}} dt \int d\vec{x} e^{-i\delta\phi(x)} w(x, X_\mu; \sigma_\mu) w(x, X_{\nu_e}; \sigma_{\nu_e}),$$

$$f = \bar{u}(\vec{p}_{\nu_\mu}) \gamma_\rho (1 - \gamma_5) u(\vec{p}_\mu) \bar{u}(\vec{p}_e) \gamma^\rho (1 - \gamma_5) u(\vec{p}_{\nu_e}),$$

$$\delta\phi(x) = \phi_\mu(x, \vec{p}_\mu) - \phi_e(x, \vec{p}_e) - \phi_{\nu_\mu}(x, \vec{p}_{\nu_\mu}) - \phi_{\nu_e}(x, \vec{p}_{\nu_e}),$$

where $\tilde{N} = 8N_\mu^{-1} N_{\nu_e}^{-1} \varrho_\mu \varrho_e \varrho_{\nu_\mu} \varrho_{\nu_e}$, for not so large $|t - T_{\nu_e}|$. For larger $|t - T_{\nu_e}|$, the spreading effect of wave packet becomes non-negligible but as was shown in Ref. [2] for the pion decay, the final result is also almost the same in the muon decay. So the spreading is not expressed explicitly in the most places. At large $|t - T_{\nu_e}|$, the wave packet vanishes at $(t - T_{\nu_e})^2 - (\vec{x} - \vec{X}_{\nu_e})^2 \leq 0$ [4], but we ignore this effect in the present paper.

C. Probability

The decay probability averaged over the initial spin and summed over the final spins of a muon of momentum p_μ , into an electron of p_e , ν_μ of p_{ν_μ} , and ν_e of p_{ν_e} is

$$\frac{1}{2} \sum_{\text{spin}} |\mathcal{M}|^2 = \frac{G_F^2}{2} \tilde{N}^2 \frac{8(p_\mu \cdot p_{\nu_e})(p_e \cdot p_{\nu_\mu})}{m_\mu m_e m_{\nu_\mu} m_{\nu_e}} |I(\delta p)|^2. \quad (43)$$

The total probability is expressed in the form,

$$P = \left(\frac{\pi^2}{\sigma_\mu \sigma_{\nu_e}}\right)^{\frac{3}{2}} \frac{2^8 G_F^2}{E_\mu (2\pi)^3} \int \frac{d\vec{p}_e d\vec{p}_{\nu_\mu} d\vec{X}_{\nu_e} d\vec{p}_{\nu_e}}{E_e E_{\nu_\mu} E_{\nu_e} (2\pi)^{12}} (p_\mu \cdot p_{\nu_e})(p_e \cdot p_{\nu_\mu}) |I(\delta p)|^2. \quad (44)$$

D. Normal term

The total probability Eq. (44) is composed of the normal term in which kinetic energy is conserved and $1/T$ -correction term. The normal term gives contributions to the value at $T \rightarrow \infty$, where $T = T_{\nu_e} - T_\mu$.

In $T \ll \tau_\mu$, the effect of the muon's life-time is negligible, and the normal term of amplitude can be computed at $T = \infty$ with the following replacement,

$$I^{\text{normal}}(\delta p) = \int_{-\infty}^{\infty} dt \int d\vec{x} e^{-i\delta\phi(x)} w(x, X_\mu; \sigma_\mu) w(x, X_{\nu_e}; \sigma_{\nu_e}). \quad (45)$$

We have

$$\begin{aligned} |I^{\text{normal}}(\delta p)|^2 &= \left(\frac{2\pi(\sigma_\mu + \sigma_{\nu_e})}{(\vec{v}_\mu - \vec{v}_{\nu_e})^2} \right) \left(\frac{2\pi\sigma_\mu\sigma_{\nu_e}}{\sigma_\mu + \sigma_{\nu_e}} \right)^3 \exp \left[-\frac{\sigma_\mu + \sigma_{\nu_e}}{(\vec{v}_\mu - \vec{v}_{\nu_e})^2} (\delta p^0 - \vec{v}_0 \cdot \delta \vec{p})^2 \right] \\ &\quad \times \exp \left[-\frac{\sigma_\mu\sigma_{\nu_e}}{\sigma_\mu + \sigma_{\nu_e}} \delta \vec{p}^2 - \frac{(\tilde{X}_\mu - \tilde{X}_{\nu_e})^2}{\sigma_\mu + \sigma_{\nu_e}} \right], \quad (46) \\ \vec{v}_0 &= \frac{\sigma_\mu \vec{v}_{\nu_e} + \sigma_{\nu_e} \vec{v}_\mu}{\sigma_\mu + \sigma_{\nu_e}}, \quad \tilde{X}_\mu = \vec{X}_\mu - \vec{v}_\mu T, \quad \tilde{X}_{\nu_e} = \vec{X}_{\nu_e} - \vec{v}_{\nu_e} T, \\ (\tilde{X}_\mu - \tilde{X}_{\nu_e})_T &= \tilde{X}_\mu - \tilde{X}_{\nu_e} - \vec{n} \left(\vec{n} \cdot (\tilde{X}_\mu - \tilde{X}_{\nu_e}) \right), \quad \vec{n} = \frac{\vec{v}_\mu - \vec{v}_{\nu_e}}{|\vec{v}_\mu - \vec{v}_{\nu_e}|}. \end{aligned}$$

The total probability of the normal term becomes

$$\begin{aligned} P^{\text{normal}} &= \frac{2^5 G_F^2}{E_\mu (\sigma_\mu \sigma_{\nu_e})^{\frac{3}{2}}} \int \frac{d\vec{p}_e d\vec{p}_{\nu_\mu} d\vec{X}_{\nu_e} d\vec{p}_{\nu_e}}{E_e E_{\nu_\mu} E_{\nu_e} (2\pi)^{12}} (p_\mu \cdot p_{\nu_e}) (p_e \cdot p_{\nu_\mu}) |I^{\text{normal}}(\delta p)|^2 \\ &= T \frac{(\sigma_\mu \sigma_{\nu_e})^{\frac{3}{2}}}{|\vec{v}_\mu - \vec{v}_{\nu_e}| (\sigma_\mu + \sigma_{\nu_e}) E_\mu (2\pi)^7} \int \frac{d\vec{p}_e d\vec{p}_{\nu_\mu} d\vec{p}_{\nu_e}}{E_e E_{\nu_\mu} E_{\nu_e}} (p_\mu \cdot p_{\nu_e}) (p_e \cdot p_{\nu_\mu}) \\ &\quad \times \exp \left[-\frac{\sigma_\mu \sigma_{\nu_e}}{\sigma_\mu + \sigma_{\nu_e}} \delta \vec{p}^2 \right] \exp \left[-\frac{\sigma_\mu + \sigma_{\nu_e}}{(\vec{v}_\mu - \vec{v}_{\nu_e})^2} (\delta p^0 - \vec{v}_0 \cdot \delta \vec{p})^2 \right]. \quad (47) \end{aligned}$$

This term is proportional to the time interval T and agrees with the asymptotic value, $T\Gamma^0 = P^0$ [1]. Therefore the asymptotic value is used for the normal term in a later section. The condition $T \ll \tau_\mu$ is satisfied in all the case of experiments analyzed in the present paper. The case of $T \approx \tau_\mu$ is given in Appendix A.

E. Finite-size corrections: spectral representation

Next, the $1/T$ -correction term is computed following the method used in Ref. [2]. For extremely large σ_μ , it is convenient to define the correlation function $\Delta_{e,\nu_\mu}(\delta x)$ with the

expression

$$\Delta_{e,\nu_\mu}(\delta x) = \frac{1}{(2\pi)^6} \int \frac{d\vec{p}_e d\vec{p}_{\nu_\mu}}{E_e E_{\nu_\mu}} (p_\mu \cdot p_{\nu_e})(p_e \cdot p_{\nu_\mu}) e^{i(p_e + p_{\nu_\mu} - p_\mu) \cdot \delta x}, \quad (48)$$

where \vec{p}_{ν_μ} and \vec{p}_e are integrated over the infinite region, $|\vec{p}_e|$ and $|\vec{p}_{\nu_\mu}| \rightarrow \infty$. The probability Eq. (44) is expressed with $\Delta_{e,\nu_\mu}(\delta x)$ as

$$P = \frac{2^5 G_F^2}{(\sigma_\mu \sigma_{\nu_e})^{\frac{3}{2}} E_\mu} \int \frac{d\vec{X}_{\nu_e} d\vec{p}_{\nu_e}}{E_{\nu_e} (2\pi)^6} \int d^4 x_1 d^4 x_2 \Delta_{e,\nu_\mu}(\delta x) e^{ip_{\nu_e} \cdot \delta x} e^{-\frac{t_1+t_2}{2\tau_\mu}} \prod_i w(x_i, X_\mu; \sigma_\mu) w(x_i, X_{\nu_e}; \sigma_{\nu_e}). \quad (49)$$

$\Delta_{e,\nu_\mu}(\delta x)$ has short-range parts that oscillate or decrease rapidly and contribute only at $|\delta \vec{x}| \approx 0$, and a long-range part. From these properties, the rate from the formers becomes constant rapidly with T , whereas the latter decreases slowly with T and gives the $1/T$ corrections. The formers contribute to the asymptotic value at $T = \infty$.

Next, we separate the long-range and shot-range parts of $\Delta_{e,\nu_\mu}(\delta x)$. We introduce a variable $Q = p_e + p_{\nu_\mu}$ and write down the integral with this new variable as

$$\begin{aligned} \Delta_{e,\nu_\mu}(\delta x) &= \int d^4 Q \delta^{(4)}(p_e + p_{\nu_\mu} - Q) \int \frac{d\vec{p}_e d\vec{p}_{\nu_\mu}}{E_e E_{\nu_\mu} (2\pi)^6} (p_\mu \cdot p_{\nu_e})(p_e \cdot p_{\nu_\mu}) e^{i(Q - p_\mu) \cdot \delta x} \\ &= \frac{1}{(2\pi)^6} \frac{1}{2} \int d^4 Q (p_\mu \cdot p_{\nu_e})(Q^2 - m_e^2) e^{i(Q - p_\mu) \cdot \delta x} F(Q), \end{aligned} \quad (50)$$

where $F(Q)$ is

$$F(Q) = \int_{-\infty}^{\infty} \frac{d\vec{p}_e d\vec{p}_{\nu_\mu}}{E_e E_{\nu_\mu}} \delta^{(4)}(p_e + p_{\nu_\mu} - Q) (p_e \cdot p_{\nu_\mu}), \quad (51)$$

and is computed in Appendix B 3 a. We have

$$\Delta_{e,\nu_\mu}(\delta x) = \frac{p_\mu \cdot p_{\nu_e}}{2(2\pi)^5} \int d^4 Q \theta(Q^0) \theta(Q^2 - m_e^2) \left(Q^2 - 2m_\mu^2 + \frac{m_e^4}{Q^2} \right) e^{i(Q - p_\mu) \cdot \delta x}. \quad (52)$$

The invariant

$$q^2 = (Q - p_\mu)^2 = Q^2 + m_\mu^2 - 2Q \cdot p_\mu \quad (53)$$

becomes, for a fixed Q^2 ,

$$q^2 \rightarrow -\infty, \quad |\vec{Q}| \rightarrow \infty. \quad (54)$$

Next, we substitute

$$\int dm^2 \delta(Q^2 - m^2) = 1 \quad (55)$$

into Eq. (52) and have the integral representation of Jost, Lehmann and Dyson [13, 14],

$$\Delta_{e,\nu_\mu}(\delta x) = \frac{p_\mu \cdot p_{\nu_e}}{2(2\pi)^2} \int_{m_e^2} dm^2 \rho(m^2) iD^+(\delta t, \delta \vec{x}; p_\mu, m), \quad (56)$$

where

$$\rho(m^2) = m^2 - 2m_e^2 + \frac{m_e^4}{m^2}, \quad (57)$$

$$iD^+(\delta t, \delta \vec{x}; p_\mu, m) = \frac{1}{(2\pi)^3} \int d^4 Q \delta(Q^2 - m^2) \theta(Q^0) e^{i(Q - p_\mu) \cdot \delta x}. \quad (58)$$

$iD^+(\delta t, \delta \vec{x}; p_\mu, m)$ is that of a relativistic particle of the mass m , which is related with Eq. (B3) in Appendix B 2, and is given as

$$\begin{aligned} m \leq m_\mu \\ iD^+(\delta t, \delta \vec{x}; p_\mu, m) &= e^{-i\delta p_\mu \cdot \delta x} \frac{1}{(2\pi)^3} \int_{Q^0=0}^{Q^0=p_\mu^0} \frac{d\vec{Q}}{2Q^0} e^{iQ \cdot \delta x} + \frac{i}{4\pi} \delta(\lambda) \epsilon(\delta t) \\ &+ \sum_{n=0}^{\infty} \frac{1}{n!} \left(\frac{\partial}{\partial \tilde{m}^2} \right)^n \left(-ip_\mu \cdot \frac{\partial}{\partial \delta x} \right)^n i\tilde{D}^+(\delta t, \delta \vec{x}; i\tilde{m}), \end{aligned} \quad (59)$$

$$m_\mu < m$$

$$iD^+(\delta t, \delta \vec{x}; p_\mu, m) = 0, \quad (60)$$

where $\tilde{D}^+(\delta t, \delta \vec{x}; i\tilde{m})$ is the sum of the Bessel functions.

Thus we have

$$\Delta_{e,\nu_\mu}(\delta x) = \frac{p_\mu \cdot p_{\nu_e}}{2(2\pi)^2} \int_{m_e^2} dm^2 \rho(m^2) \left(i \frac{\epsilon(\delta t)}{4\pi} \delta(\lambda) + \text{“Normal”} + J_{\text{regular}} \right). \quad (61)$$

The first term and the rests in the right-hand side of Eq. (61) contribute to the leading finite-size correction, and those of short-distance regions of Eq. (49), respectively.

The sum of J_{regular} and the light-cone singular term do not contribute to the asymptotic value, because these terms come from the integral over momentum outside the physical region. The power series in J_{regular} of Eq. (61) converges in the region [2],

$$2p_\mu \cdot p_{\nu_e} \leq m_\mu^2 - m^2, \quad (62)$$

and the light-cone singularity of the form $\delta(\lambda)\epsilon(\delta t)$ appears only in the region, Eq. (62).

The probability is written in the form

$$\begin{aligned} P &= \frac{2^5 G_F^2}{(\sigma_\mu \sigma_{\nu_e})^{\frac{3}{2}} E_\mu} \int \frac{d\vec{X}_{\nu_e} d\vec{p}_{\nu_e}}{E_{\nu_e} (2\pi)^6} \frac{p_\mu \cdot p_{\nu_e}}{2(2\pi)^2} \int_{m_e^2}^{m_\mu^2 - p_\mu \cdot p_{\nu_e}} dm^2 \rho(m^2) \\ &\times \int d^4 x_1 d^4 x_2 iD^+(\delta t, \delta \vec{x}; p_\mu, m) e^{ip_{\nu_e} \cdot \delta x} e^{-\frac{t_1 + t_2}{\tau_\mu}} \prod_{i=1,2} w(x_i, X_\mu; \sigma_\mu) w(x_i, X_{\nu_e}; \sigma_{\nu_e}). \end{aligned} \quad (63)$$

For $i\frac{\epsilon(\delta t)}{4\pi}\delta(\lambda)$ in $iD^+(\delta t, \delta\vec{x}; p_\mu, m)$ and $\sigma_\mu \gg \sigma_{\nu_e}$, we have

$$\begin{aligned} & \int d\vec{X}_{\nu_e} \int d^4x_1 d^4x_2 e^{ip_{\nu_e} \cdot \delta x} e^{-\frac{1}{4\sigma_\mu}(\delta\vec{x} - \vec{v}_\mu \delta t)^2 - \frac{1}{4\sigma_{\nu_e}}(\delta\vec{x} - \vec{v}_{\nu_e} \delta t)^2} i\frac{\epsilon(\delta t)}{4\pi}\delta(\lambda) \\ & \quad \times \prod_{i=1,2} w(x_i, X_\mu; \sigma_\mu) w(x_i, X_{\nu_e}; \sigma_{\nu_e}) \\ & = \frac{i\sigma_{\nu_e}(\pi^2\sigma_\mu\sigma_{\nu_e})^{\frac{3}{2}}}{2} \int_0^T dt_1 dt_2 e^{-\frac{(\vec{v}_{\nu_e} - \vec{v}_\mu)^2 \delta t^2}{4\sigma_\mu}} e^{-\frac{t_1+t_2}{2\tau_\mu}} \frac{e^{i(\omega_{\nu_e} \delta t)}}{\delta t}, \end{aligned} \quad (64)$$

where $\omega_{\nu_e} = \frac{m_{\nu_e}^2}{2E_{\nu_e}}$, and details and general cases of integral with $f(\delta x)$ are given in Appendix C. The integral in t_1 and t_2 in Eq. (64) is computed easily in two extremum cases,

$$0, \text{ for } \frac{4\sigma_\mu}{(\vec{v}_\mu - \vec{v}_{\nu_e})^2} = \text{microscopic}, \quad (65)$$

$$\tau_\mu \{ \tilde{g}(\omega_{\nu_e}, T; \tau_\mu) - g(\omega_{\nu_e}, \infty; \tau_\mu) \}, \text{ for } \frac{4\sigma_\mu}{(\vec{v}_\mu - \vec{v}_{\nu_e})^2} = \infty, \quad (66)$$

where $\tilde{g}(\omega_{\nu_e}, T; \tau_\mu)$ and $g(\omega_{\nu_e}, \infty; \tau_\mu)$ are also given in Appendix C. The second term in the right-hand side of Eq. (66) is cancelled with J_{regular} . So the wave functions of the initial and final states overlap in wide area for $\sigma_\mu \rightarrow \infty$, and the probability has corrections.

For $\sigma_\mu \approx \infty$, the probability is composed of the finite-size correction and the normal term:

$$P = \frac{2G_F^2}{E_\mu} \int \frac{d\vec{p}_{\nu_e} p_\mu \cdot p_{\nu_e}}{E_{\nu_e} (2\pi)^5} \int dm^2 \rho(m^2) [\sigma_{\nu_e} \mathcal{C} \tilde{g}(\omega_{\nu_e}, T; \tau_\mu) + \text{“Normal”}], \quad (67)$$

where

$$\int_{m_e^2}^{m_\mu^2 - 2p_\mu \cdot p_{\nu_e}} dm^2 \rho(m^2) \simeq \frac{(m_\mu^2 - 2p_\mu \cdot p_{\nu_e})^2}{2} \theta(m_\mu^2 - 2p_\mu \cdot p_{\nu_e}), \quad (68)$$

$$(69)$$

and \mathcal{C} is constant in p_{ν_e} and given in Appendix C for various cases. In the above derivation, we used Eq. (62) and ignored m_e . Then, we have the rate

$$P = T\Gamma^0 + P^{(d)}, \quad (70)$$

$$P^{(d)} = \mathcal{C} \frac{G_F^2}{E_\mu} \int \frac{d\vec{p}_{\nu_e}}{E_{\nu_e} (2\pi)^5} (p_\mu \cdot p_{\nu_e}) (m_\mu^2 - 2p_\mu \cdot p_{\nu_e})^2 \theta(m_\mu^2 - 2p_\mu \cdot p_{\nu_e}) \sigma_{\nu_e} \tilde{g}(\omega_{\nu_e}, T; \tau_\mu). \quad (71)$$

We have the integral over the phase space:

$$\tilde{J}(p_\mu) = 2\pi\mathcal{C} \int |\vec{p}_{\nu_e}| d|\vec{p}_{\nu_e}| d\cos\theta \left[\theta(m_\mu^2 - 2p_\mu \cdot p_{\nu_e}) (p_\mu \cdot p_{\nu_e}) (m_\mu^2 - 2p_\mu \cdot p_{\nu_e})^2 \sigma_{\nu_e} \tilde{g}(\omega_{\nu_e}, T; \tau_\mu) \right], \quad (72)$$

where θ is the angle between the momenta of μ and ν_e . From the convergence condition, $\cos \theta$ satisfies

$$\cos \theta \leq \cos \theta_c = \frac{E_\mu}{|\vec{p}_\mu|} - \frac{m_\mu^2}{2|\vec{p}_\mu||\vec{p}_{\nu_e}|}, \quad (73)$$

and agrees with

$$\cos \theta_c = \pm 1 \quad (74)$$

at

$$E_{\max} = \frac{m_\mu^2}{2(E_\mu - |\vec{p}_\mu|)}, \quad E_{\min} = \frac{m_\mu^2}{2(E_\mu + |\vec{p}_\mu|)}. \quad (75)$$

Hence in the region

$$E_{\nu_e} \leq E_{\min}, \quad (76)$$

$\cos \theta$ in Eq. (72) is integrated over $-1 \leq \cos \theta \leq 1$, and we have

$$\tilde{J}_1(p_\mu) = \frac{2\pi\mathcal{C}\sigma_{\nu_e}}{|\vec{p}_\mu|} \int_0^{E_{\min}} dE_{\nu_e} F_1(E_{\nu_e}) \tilde{g}(\omega_{\nu_e}, T; \tau_\mu), \quad (77)$$

$$F_1(E_{\nu_e}) = E_{\nu_e}^2 \left[E_{\nu_e}^2 (p_\mu^{+4} - p_\mu^{-4}) - \frac{4}{3} E_{\nu_e} m_\mu^2 (p_\mu^{+3} - p_\mu^{-3}) + \frac{m_\mu^4}{2} (p_\mu^{+2} - p_\mu^{-2}) \right], \quad (78)$$

where

$$|\vec{p}_{\nu_e}| \sim E_{\nu_e}, \quad p_\mu^+ = E_\mu + |\vec{p}_\mu|, \quad p_\mu^- = E_\mu - |\vec{p}_\mu|. \quad (79)$$

In the region

$$E_{\min} \leq E_{\nu_e} \leq E_{\max}, \quad (80)$$

$\cos \theta$ in Eq. (72) is integrated over $\cos \theta_c \leq \cos \theta \leq 1$:

$$\tilde{J}_2(p_\mu) = \frac{2\pi\mathcal{C}\sigma_{\nu_e}}{|\vec{p}_\mu|} \int_{E_{\min}}^{E_{\max}} dE_{\nu_e} F_2(E_{\nu_e}) \tilde{g}(\omega_{\nu_e}, T; \tau_\mu), \quad (81)$$

$$F_2(E_{\nu_e}) = E_{\nu_e}^2 \left[E_{\nu_e}^2 \left\{ p_\mu^{-4} - \left(\frac{m_\mu^2}{2E_{\nu_e}} \right)^4 \right\} - \frac{4}{3} E_{\nu_e} m_\mu^2 \left\{ p_\mu^{-3} - \left(\frac{m_\mu^2}{2E_{\nu_e}} \right)^3 \right\} + \frac{m_\mu^4}{2} \left\{ p_\mu^{-2} - \left(\frac{m_\mu^2}{2E_{\nu_e}} \right)^2 \right\} \right]. \quad (82)$$

Finally, the probability $P^{(d)}$ is written as

$$\begin{aligned} P^{(d)} &= \frac{G_F^2}{(2\pi)^5 E_\mu} \left(\tilde{J}_1(p_\mu) + \tilde{J}_2(p_\mu) \right) \\ &= \frac{G_F^2 \sigma_{\nu_e} \mathcal{C}}{(2\pi)^4 E_\mu |\vec{p}_\mu|} \left[\int_0^{E_{\min}} dE_{\nu_e} F_1(E_{\nu_e}) \tilde{g}(\omega_{\nu_e}, T; \tau_\mu) + \int_{E_{\min}}^{E_{\max}} dE_{\nu_e} F_2(E_{\nu_e}) \tilde{g}(\omega_{\nu_e}, T; \tau_\mu) \right]. \end{aligned} \quad (83)$$

F. Energy spectrum

1. Diffraction component

The energy spectrum of the diffraction component is given by

$$\begin{aligned}
P^{(d)} &= \frac{G_F^2}{(2\pi)^5 E_\mu} \tilde{J}(p_\mu), \\
\tilde{J}(p_\mu) &= \frac{2\pi\sigma_{\nu_e}\mathcal{C}}{|\vec{p}_\mu|} \int dE_{\nu_e} [F_1(E_{\nu_e})\tilde{g}(\omega_{\nu_e}, T; \tau_\mu)\theta(E_{\min} - E_{\nu_e}) \\
&\quad + F_2(E_{\nu_e})\tilde{g}(\omega_{\nu_e}, T; \tau_\mu)\theta(E_{\max} - E_{\nu_e})\theta(E_{\nu_e} - E_{\min})], \\
\frac{dP^{(d)}}{dE_{\nu_e}} &= \frac{G_F^2\sigma_{\nu_e}\mathcal{C}}{(2\pi)^4 E_\mu |\vec{p}_\mu|} [F_1(E_{\nu_e})\tilde{g}(\omega_{\nu_e}, T; \tau_\mu)\theta(E_{\min} - E_{\nu_e}) \\
&\quad + F_2(E_{\nu_e})\tilde{g}(\omega_{\nu_e}, T; \tau_\mu)\theta(E_{\max} - E_{\nu_e})\theta(E_{\nu_e} - E_{\min})].
\end{aligned} \tag{84}$$

For the low-energy muon $|\vec{p}_\mu| \ll E_\mu \sim m_\mu$,

$$F_1(E_{\nu_e}) = |\vec{p}_\mu| \frac{m_\mu^7}{2} x^2 (1-x)^2, \quad F_2(E_{\nu_e}) = 0, \quad x = \frac{2E_{\nu_e}}{m_\mu}, \tag{86}$$

and

$$\frac{dP^{(d)}}{dx} = \frac{G_F^2\sigma_{\nu_e}\mathcal{C}m_\mu^7}{4(2\pi)^4} x^2 (1-x)^2 \tilde{g}(\omega_{\nu_e}, T; \tau_\mu) \theta\left(\frac{m_\mu}{2} - E_{\nu_e}\right). \tag{87}$$

Equation (87) is different from the spectrum at asymptotic region, Eq. (28). There is no precise data even for the electron in $x < 1/2$, by now. Our predictions are given in Fig. 3 with a suitable value of σ_{ν_e} at $cT = 1\text{m}$ and 10 m . Because the infinite-momentum states of positive energy contribute to the diffraction term, kinetic energy of detected particle becomes smaller than that of asymptotic region and the peak of spectrum shifts to a value lower than that of the normal term. It would be interesting to confirm this component. The effect is reduced if the muon is not a plane wave but a small wave packet. Low-energy-negative muon in matter is trapped to an atom and forms a bound state of a small wave function.

2. Normal component

From Eq. (28), the energy dependence of normal component of μDAR at asymptotic region is written as

$$\frac{dP^0}{dx} = \frac{G_F^2 m_\mu^5}{2(2\pi)^3} x^2 (1-x) \tau_\mu (1 - e^{-\frac{T_D}{\tau_\mu}}), \tag{88}$$

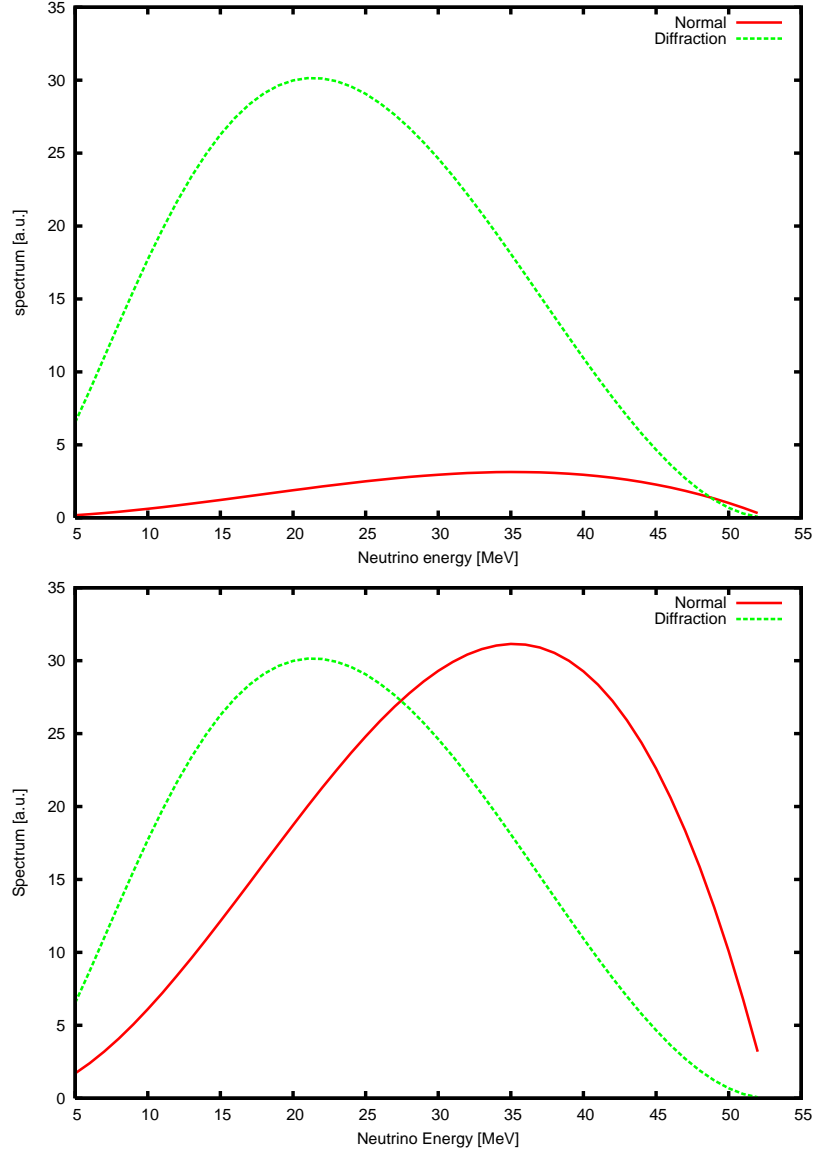


FIG. 3. (Color online) ν_e spectrum in μ DAR. The red curve shows normal component given in Eq. (88) and green curve shows diffraction component given in Eq. (87). $m_{\nu_e} = 0.08$ eV, and $2\sigma_{\nu_e} = 12^{\frac{2}{3}}/m_\pi^2$ (^{12}C carbon target) are used for numerical computation. Here, detector is located at $L = 0$. The top figure is for $cT = cT_D = 1$ and bottom one is for $cT = cT_D = 10$ m.

where T_D is a depth of detector. For μ DAR, the depth of the detector determines the time width. For μ DIF, a decay region cT restricts the time width where μ exists. They are used properly according to experimental conditions. The normal component of transition rate or probability is independent of the size of wave packets from the completeness, but the energy spectrum depends on it and varies with the size. The spectrum for plane wave given in Eq. (28) was confirmed in the electron spectrum in the upper-energy region $x \geq 1/2$.

G. Mean life-time at a finite distance

The total probability becomes larger than the asymptotic value due to the diffraction component in small T , and the average life-time measured by detecting the neutrino in final states there becomes shorter than the asymptotic value, Eq. (27).

H. Size of neutrino wave packet

Particles and anti-particles are treated equally so far, but we should be careful to consider the boundary conditions of experiment [12]. For example, when ν_e is detected by using $^{12}C + \nu_e \rightarrow ^{12}N_{g.s.} + e^-$ process, the target nucleus is ^{12}C and its size is $12^{\frac{1}{3}}/m_\pi$. So we use this size for σ_{ν_e} as

$$2\sigma_{\nu_e} = \frac{12^{\frac{2}{3}}}{m_\pi^2}. \quad (89)$$

$\bar{\nu}_e$ is detected by inverse beta decay and delayed signal of neutron capture. In this process, the lightest nucleus 1H i.e., proton can be a target and its wave function expands due to center of gravity effect [2]. From Eq. (83), the diffraction term is proportional to σ_{ν_e} or $\sigma_{\bar{\nu}_e}$. According to these properties, the diffraction term for $\bar{\nu}_e$ can become larger than that for ν_e when a light nucleus contributes to the detection process. When $C_n H_{2n+2}$ is used for scintillator, the size of wave packet is calculated from the ratio of proton between C and H , and is written as

$$2\sigma_{\bar{\nu}_e} = \frac{3}{4} \frac{12^{\frac{2}{3}}}{m_\pi^2} + \frac{1}{4} \left(\frac{m_e a_\infty}{m_p + m_e} \right)^2, \quad (90)$$

where m_e and m_p are masses of electron and proton, and a_∞ is Bohr radius. If the detector consists of a mixture of several materials, the wave packet size becomes the value averaged over the abundance ratio of materials.

At $T \rightarrow 0$, the diffraction term is proportional to T , and it may be possible to determine σ_ν experimentally by using this feature [12].

I. Mixing effect on diffraction term

So far the mixing of neutrino is ignored to make the points of the corrections clear, but it is found that the diffraction term depends on m_ν and is sensitive to the difference of mass

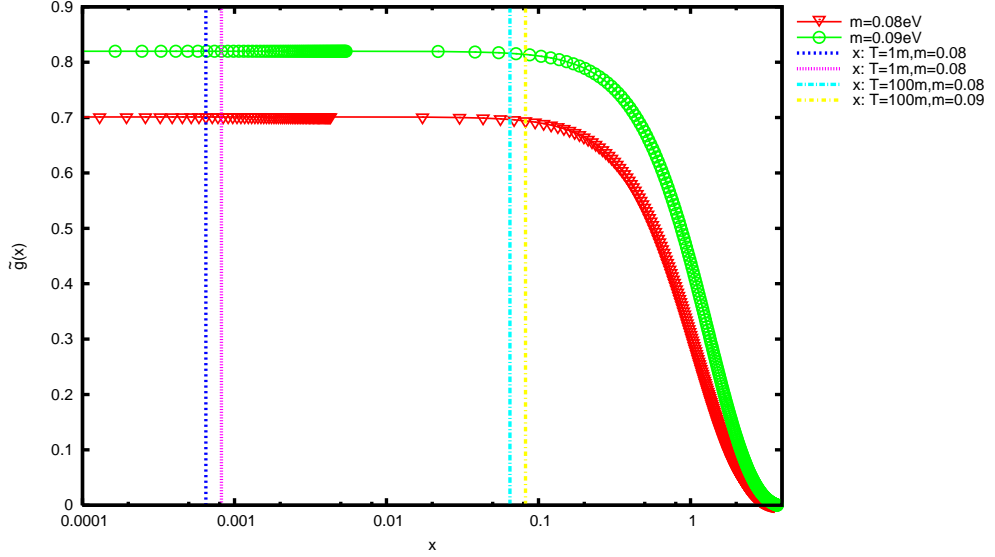


FIG. 4. (Color online) $\tilde{g}_{e,e}(\omega_{\nu_e}, T; \tau_\mu)$ of including flavor mixing, Eq. (96), is shown. The horizontal axis is $x = \omega_{\nu_h} T$, where $\omega_{\nu_h} = \frac{m_{\nu_h}^2}{2E_{\nu_e}}$, and m_{ν_h} is the mass of heaviest neutrino and $E_\nu = 25$ MeV. Inverted hierarchy is assumed and $m_{\nu_h} = m_{\nu_2} = 0.08$ (red), 0.09 (green) eV are used. Dashed lines correspond to x values for $cT = 1$ m, $m_{\nu_2} = 0.08$ eV (blue), $m_{\nu_2} = 0.09$ eV (magenta), and $cT = 100$ m, $m_{\nu_2} = 0.08$ eV (light blue), $m_{\nu_2} = 0.09$ eV (yellow), respectively.

of the order of 0.1 eV or less [15]. Consequently, this dependence gives a new mixing effect that is very different from usual flavor oscillation. The present mixing effect appears in short distance region, whereas the flavour oscillation appears in long distance region. From here the mixing matrix $U_{\alpha,i}$ is included, and the effect of the mixing to the diffraction term is studied. With three mass eigen states of neutrino of m_{ν_i} , $i = 1 - 3$ and $U_{\alpha,i}$, the flavor neutrino fields $\nu_l(x)$ in Eq. (5) are the linear combination of the fields of three $\nu_i(x)$ having mass m_i as

$$\nu_l(x) = \sum_i U_{l,i} \nu_i(x), \quad l = e, \mu, \tau, \quad (91)$$

where the best-fit values of mixing angles given by [5]

$$\begin{aligned} \sin \theta_{12} &= 0.307^{+0.018}_{-0.016}, \\ \sin \theta_{13} &= 0.386^{+0.024}_{-0.021}, \\ \sin \theta_{23} &= 0.0241 \pm 0.0025, \end{aligned} \quad (92)$$

$$(93)$$

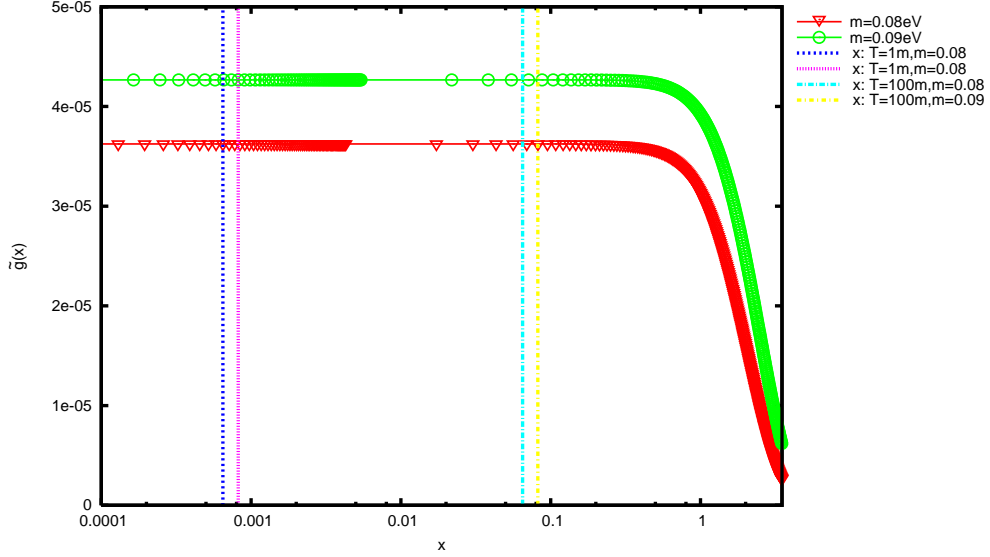


FIG. 5. (Color online) $\tilde{g}_{\mu,e}(\omega_{\nu_e}, T; \tau_\mu)$ of including flavor mixing, Eq. (96), is shown. The horizontal axis is $x = \omega_{\nu_h} T$, where $\omega_{\nu_h} = \frac{m_{\nu_h}^2}{2E_{\nu_e}}$, and m_{ν_h} is the mass of heaviest neutrino and $E_\nu = 25$ MeV. Inverted hierarchy is assumed and $m_{\nu_h} = m_{\nu_2} = 0.08$ (red), 0.09 (green) eV are used. Dashed lines correspond to x values for $cT = 1$ m, $m_{\nu_2} = 0.08$ eV (blue) and $m_{\nu_2} = 0.09$ eV (magenta), and for $cT = 100$ m, $m_{\nu_2} = 0.08$ eV (light blue) and $m_{\nu_2} = 0.09$ eV (yellow), respectively.

are used and CP violation phase $\delta_{CP} = 0$ is assumed. The amplitude for the anti-neutrino of flavor α to be detected in μ^+ decay ($\mu^+ \rightarrow \bar{\nu}_\mu + e^+ + \nu_e$) is

$$\mathcal{M}_{\alpha,\mu} = \sum_i U_{\alpha,i} \mathcal{M}(\mu^+, i) U_{\mu,i}^*, \quad (94)$$

or the amplitude for the neutrino of flavor α' in μ^+ decay ($\mu^+ \rightarrow \bar{\nu}_\mu + e^+ + \underline{\nu}_e$) is

$$\mathcal{M}'_{\alpha',e} = \sum_i U_{\alpha',i} \mathcal{M}'(\mu^+, i) U_{e,i}^*. \quad (95)$$

Then, the amplitude for a flavor change from α to β is proportional to a new universal function $\tilde{g}_{\alpha,\beta}(\omega_{\nu_\alpha}, T; \tau_\mu)$ as

$$\mathcal{M}_{\alpha,\beta} \propto \tilde{g}_{\alpha,\beta}(\omega_{\nu_\beta}, T; \tau_\mu) = \sum_{i,j} U_{\beta,i} U_{\alpha,i}^* U_{\beta,j}^* U_{\alpha,j} \tilde{g}(\omega_i, \omega_j, T; \tau_\mu). \quad (96)$$

The behaviors of new $\tilde{g}_{\alpha,\beta}(\omega_{\nu_\beta}, T; \tau_\mu)$ of $\alpha = \beta = e$ and $\alpha = \mu$, and $\beta = e$ are shown in Figs. 4 and 5. From these figures, we can see that $\tilde{g}_{e,e}(\omega_{\nu_e})$ and $\tilde{g}_{\mu,e}(\omega_{\nu_e})$ are almost constant at $T < 100$ m but the magnitude is sensitive to the absolute neutrino mass. So, there is a wide window where the absolute neutrino mass can be measured by using the finite-size

corrections. Furthermore, $\tilde{g}_{\mu,e}(\omega_{\nu_e})$ is much smaller than $\tilde{g}_{e,e}(\omega_{\nu_e})$ but does not vanish and causes a new flavor changing effect on neutrino. Implications of this effect will be discussed in the next section, and more details about $\tilde{g}_{\alpha,\beta}$ are given in Appendix C.

IV. IMPLICATIONS TO NEUTRINO EXPERIMENTS

According to previous section, the finite-size corrections to the probabilities of the events that neutrinos are detected in muon decay can be large and show peculiar flavor changes. For π decay it was found that the corrections is sizable and important to neutrinos at short distance [1, 2, 15]. In this section, we analyze the finite-size corrections to muon decays in several experiments and complete the analyses. Including the effects from the detection process and the mixing of neutrino, neutrino and anti-neutrino have different behaviors on the diffraction term. So they should be treated distinctively in accord with the experimental conditions.

At ground experiments, μ^+ (μ^-) is produced in π^+ (π^-) decay simultaneously with a ν_μ ($\bar{\nu}_\mu$) first, and decays to e^+ (e^-), $\bar{\nu}_\mu$ (ν_μ) and ν_e ($\bar{\nu}_e$). There are typical two types of ground experiments in which the finite-size corrections to neutrinos in muon decay are important. One is the accelerator experiment that uses a neutrino beam from pion decay. In this case, both decays of high-energy π and μ are source of neutrinos and can have the finite-size corrections. The other is the experiment that observes $\bar{\nu}_e$ or ν_μ appearance in μ^+ decay. In this experiment μ^+ is extracted and used as a source of neutrino, and π is not involved.

Hereafter, we focus only on μ^+ decay and study the finite-size corrections in the above two types of experiments, and compare with the existing results. We also give predictions for future experiments. They would supply the absolute neutrino mass and the information on hierarchy of neutrino masses. As was discussed in Sec. II B, parent μ^+ do not form bound states in matter and are assumed to be approximated with plane waves in both cases.

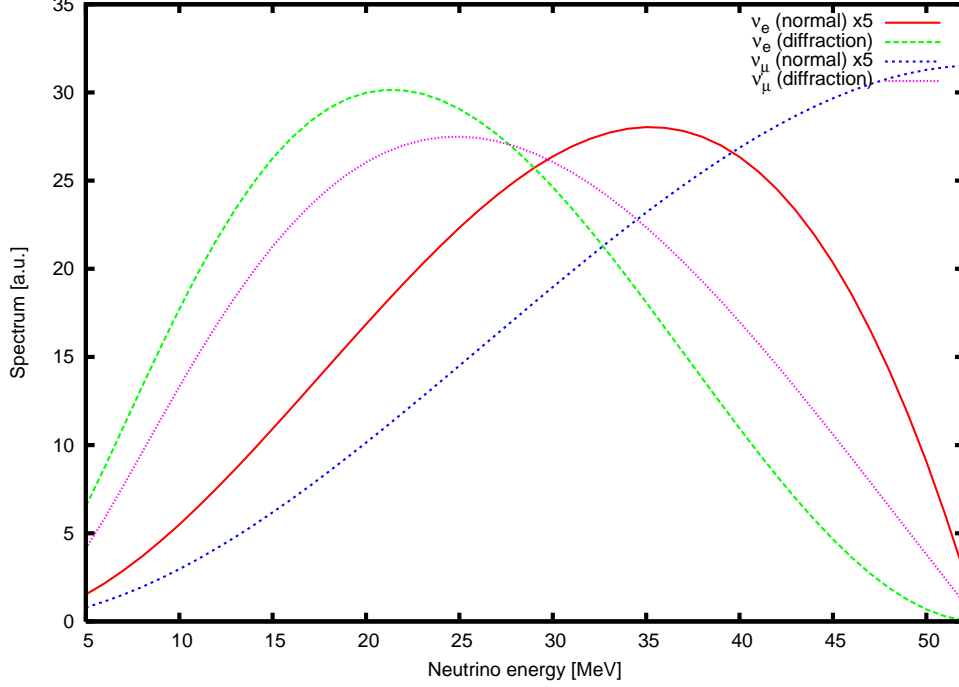


FIG. 6. (Color online) Spectra of normal and diffraction terms for ν_e and $\bar{\nu}_\mu$ in μ^+ DAR are shown. Spectra of normal terms for ν_e (red) and $\bar{\nu}_\mu$ (blue) are different from those of ν_e (green) and $\bar{\nu}_\mu$ (magenta). These properties can be used to eliminate background events from μ^- decays, and so on. $m_{\nu_h} = 0.08$ eV, $\sigma_\nu = 12^{\frac{2}{3}}/m_\pi^2$, $cT = cT_D = 1.0$ m, and inverted hierarchy is assumed in numerical calculation.

A. ν_e and $\bar{\nu}_\mu$ in μ^+ decay

1. μ^+ decay at rest (μ^+ DAR)

In μ^+ DAR, only ν_e is observable and $\bar{\nu}_\mu$ cannot be observed in charged current interactions. However, in order to distinguish background events or the flavor oscillation phenomena, spectrum of $\bar{\nu}_\mu$ is also important. Both ν_e and $\bar{\nu}_\mu$ have finite-size corrections, and the spectra of normal and diffraction terms for $\bar{\nu}_\mu$ are

$$\frac{dP^0}{dE_{\bar{\nu}_\mu}} = \frac{G_F^2 m_\mu^2}{12\pi^3} E_{\bar{\nu}_\mu}^2 \left(3 - 4 \frac{E_{\bar{\nu}_\mu}}{m_\mu} \right) \tau_\mu \left(1 - e^{-\frac{T_D}{\tau_\mu}} \right), \quad (97)$$

$$\frac{dP^{(d)}}{dE_{\bar{\nu}_\mu}} = \frac{G_F^2 m_\mu^2}{12\pi^3} \frac{E_{\bar{\nu}_\mu}^2 m_\mu^2 \sigma_{\bar{\nu}_\mu}}{4\pi} \left(1 - 2 \frac{E_{\bar{\nu}_\mu}}{m_\mu} \right) \left(5 - 6 \frac{E_{\bar{\nu}_\mu}}{m_\mu} \right) \tau_\mu \tilde{g}(\omega_{\bar{\nu}_\mu}, T; \tau_\mu), \quad (98)$$

and a ratio of them are

$$\begin{aligned}
R(E_{\bar{\nu}_\mu}) &= \frac{dP^0}{dE_{\bar{\nu}_\mu}} \bigg/ \frac{dP^{(d)}}{dE_{\bar{\nu}_\mu}} \\
&= \frac{m_\mu^2 \sigma_{\bar{\nu}_\mu}}{4\pi} \frac{\left(1 - 2\frac{E_{\bar{\nu}_\mu}}{m_\mu}\right) \left(5 - 6\frac{E_{\bar{\nu}_\mu}}{m_\mu}\right)}{3 - 4\frac{E_{\bar{\nu}_\mu}}{m_\mu}} \frac{\tilde{g}(\omega_{\bar{\nu}_\mu}, T; \tau_\mu)}{1 - e^{-\frac{T_D}{\tau_\mu}}}.
\end{aligned} \tag{99}$$

As is the case with the spectrum of diffraction term for ν_e , the spectrum Eq. (98) gives lower energy components.

The spectra of diffraction and normal terms for ν_e are given in Eqs. (87) and (88) and ratio of them are

$$R(E_{\nu_e}) = \frac{\sigma_{\nu_e} m_\mu^2 \left(1 - \frac{2E_{\nu_e}}{m_\mu}\right)}{4\pi (1 - \exp[-T_D/\tau_\mu])} \tilde{g}_{e,e}(\omega_{\nu_e}, T; \tau_\mu), \tag{100}$$

Figure 6 shows the spectra Eqs. (87), (88), (97), and (98). Since the shapes of each spectrum are different, it is possible to distinguish the background events and the oscillation phenomena from the finite-size corrections. The magnitude of the correction depends on T , m_ν and σ_{ν_e} . According to Fig. 6, the ratios Eqs. (99) and (100) are about 5 at $cT = cT_D = 1$ m with $m_{\nu_h} = 0.08$ eV of inverted hierarchy. This value is quite large compared with that of π decay [15]: if it is possible to identify ν_e from μ^+ DAR and collect sufficient statistics, it may be feasible to observe the finite-size correction as the excess of ν_e flux and measure the absolute neutrino mass.

2. μ^+ decay in flight (μ^+ DIF)

In μ^+ DIF, the spectra of ν_e for the normal and diffraction terms are

$$\frac{d^2 P_{\nu_e}^0}{dE_{\nu_e} d\cos\theta} = \frac{2G_F^2 E_{\nu_e}^2}{(2\pi)^3 E_\mu} (E_\mu - p_\mu \cos\theta) (m_\mu^2 - 2p_\mu \cdot p_{\nu_e}) \gamma \tau_\mu \left(1 - \exp\left[-\frac{T}{\gamma \tau_\mu}\right]\right), \tag{101}$$

$$\frac{d^2 P_{\nu_e}^{(d)}}{dE_{\nu_e} d\cos\theta} = \frac{G_F^2 E_{\nu_e}^2}{(2\pi)^4 E_\mu} (E_\mu - p_\mu \cos\theta) (m_\mu^2 - 2p_\mu \cdot p_{\nu_e})^2 \sigma_{\nu_e} \gamma \tau_\mu \tilde{g}_{e,e}(\omega_{\nu_e}, T; \gamma \tau_\mu), \tag{102}$$

where θ is an angle between \vec{p}_μ and $\vec{p}_{\bar{\nu}_\mu}$, and $\gamma = E_\mu/m_\mu$. The spectrum of normal term of $\bar{\nu}_\mu$ from high-energy μ^+ is

$$\begin{aligned}
\frac{d^2 P_{\bar{\nu}_\mu}^0}{dE_{\bar{\nu}_\mu} d\cos\theta} &= \frac{G_F^2 E_{\bar{\nu}_\mu}^2}{24\pi^3 E_\mu} [(E_\mu - p_\mu \cos\theta)(3m_\mu^2 - 4E_{\bar{\nu}_\mu}(E_\mu - p_\mu \cos\theta))] \\
&\quad \times \gamma \tau_\mu \left(1 - \exp\left[-\frac{T}{\gamma \tau_\mu}\right]\right),
\end{aligned} \tag{103}$$

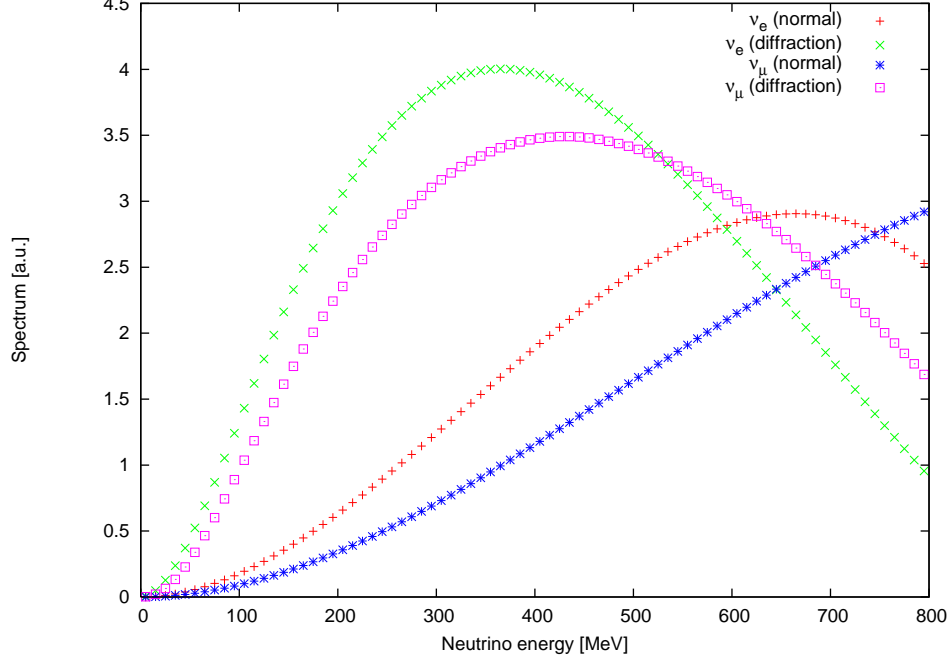


FIG. 7. (Color online) Spectra of normal and diffraction terms for ν_e and $\bar{\nu}_\mu$ in μ^+ DIF are shown. Spectra of normal terms for ν_e (red) and $\bar{\nu}_\mu$ (blue) are different from those of ν_e (green) and $\bar{\nu}_\mu$ (magenta). These properties can be used to eliminate back ground events from μ^- decays, and so on. $m_{\nu_h} = 0.08$ eV, $\sigma_\nu = 12^{\frac{2}{3}}/m_\pi^2$, $cT = 200$ m, $\cos \theta = 1$, and $E_\mu = 1$ GeV are used, and inverted hierarchy is assumed in numerical calculation.

and that of diffraction term is

$$\begin{aligned} \frac{d^2 P_{\bar{\nu}_\mu}^{(d)}}{dE_{\bar{\nu}_\mu} d\cos\theta} &= \frac{G_F^2}{24\pi^3 E_\mu} \frac{E_{\bar{\nu}_\mu}^2}{4\pi} (E_\mu - p_\mu \cos\theta) (m_\mu^2 - 2E_{\bar{\nu}_\mu} (E_\mu - p_\mu \cos\theta)) \\ &\quad \times (5m_\mu^2 - 6E_{\bar{\nu}_\mu} (E_\mu - p_\mu \cos\theta)) \gamma\tau_\mu \sigma_{\bar{\nu}_\mu} \tilde{g}_{\mu,\mu}(\omega_{\bar{\nu}_\mu}, T; \gamma\tau_\mu). \end{aligned} \quad (104)$$

The spectra Eqs. (101)–(104) are shown in Fig. 7.

The ratios between normal and diffraction terms for ν_e and $\bar{\nu}_\mu$ are

$$R(E_{\nu_e}, \cos\theta) = \frac{\sigma_{\nu_e}}{4\pi} (m_\mu^2 - 2E_{\nu_e} (E_\mu - p_\mu \cos\theta)) \frac{\tilde{g}_{e,e}(\omega_{\nu_e}, T; \gamma\tau_\mu)}{1 - \exp[-T/\gamma\tau_\mu]}, \quad (105)$$

$$R(E_{\bar{\nu}_\mu}, \cos\theta) = \frac{\sigma_{\bar{\nu}_\mu}}{4\pi} \frac{(m_\mu^2 - 2E_{\bar{\nu}_\mu} (E_\mu - p_\mu \cos\theta)) (5m_\mu^2 - 6E_{\bar{\nu}_\mu} (E_\mu - p_\mu \cos\theta))}{3m_\mu^2 - 4E_{\bar{\nu}_\mu} (E_\mu - p_\mu \cos\theta)} \frac{\tilde{g}_{\mu,\mu}(\omega_{\bar{\nu}_\mu}, T; \gamma\tau_\mu)}{(1 - \exp[-T/\gamma\tau_\mu])}. \quad (106)$$

According to Fig. 7, $R(E_{\bar{\nu}_\mu})$ and $R(E_{\nu_e})$ for on-axis $\bar{\nu}_\mu$ and ν_e are about unity with $E_\mu = 1$ GeV, $m_{\nu_h} = 0.08$ eV of inverted hierarchy, and σ_ν of nuclear size at $cT = 200$ m. Even if the flux of parent muon is small, this effect is not negligible and may be observed at high-energy

neutrino experiments. Our effects will be compared with existing experimental results in the next section.

3. *Excess of electron neutrino in accelerator experiments*

To study the flavor oscillation phenomena, accelerator neutrino experiments use a neutrino beam produced by π decays and search an excess in electron neutrino mode. In π^+ decay, ν_e is produced in processes

$$\pi^+ \rightarrow \mu^+ + \nu_\mu, \quad (107)$$

$$\mu^+ \rightarrow e^+ + \bar{\nu}_\mu + \underline{\nu_e}, \quad (108)$$

$$\rightarrow e^+ + \underline{\nu_e}, \quad (109)$$

and has two sources. The probability to detect neutrinos in π decay and that in μ decay have the finite-size corrections. We already compared the correction to ν_e in π^+ decay with the existing data of MiniBooNE [18] and found that the corrections to ν_e events are consistent but are not satisfactory to explain the experimental results [15]. To complete the analysis, we should include the correction to ν_e in μ^+ decay. Since μ^+ is the second particle produced by π^+ decay, its decay region is reduced by the distance where the parent π^+ travels until its decay. This effect of pion's finite life-time is also included to compute the finite-size correction.

MiniBooNE experiment [18] reported the appearance of ν_e and $\bar{\nu}_e$ in ν_μ or $\bar{\nu}_\mu$ beam produced by π^\pm decay. The normal mode of muon decay, Eq. (108), has been estimated with Monte Carlo simulation as background and used, but the diffraction mode has not included in the analysis. We computed the diffraction mode under the MiniBooNE experimental condition. It is found that the correction to ν_e from π^+ decay, Eq. (109) [15] but that of ν_e from μ^+ , Eq. (108) is large in the present work. Figure 8 shows the comparison of our numerical results of ratio between normal and diffraction modes with the data. From this figure, the finite-size correction in μ^+ decay dominates in ν_e events at MiniBooNE experiments, and is sensitive to the absolute mass value of neutrino and mass hierarchy. Our results are consistent within errors of the experiment and Monte Carlo simulation with the absolute neutrino mass values of $m_{\nu_h} = 0.07 - 0.08$ eV. This is consistent with our previous results [15].

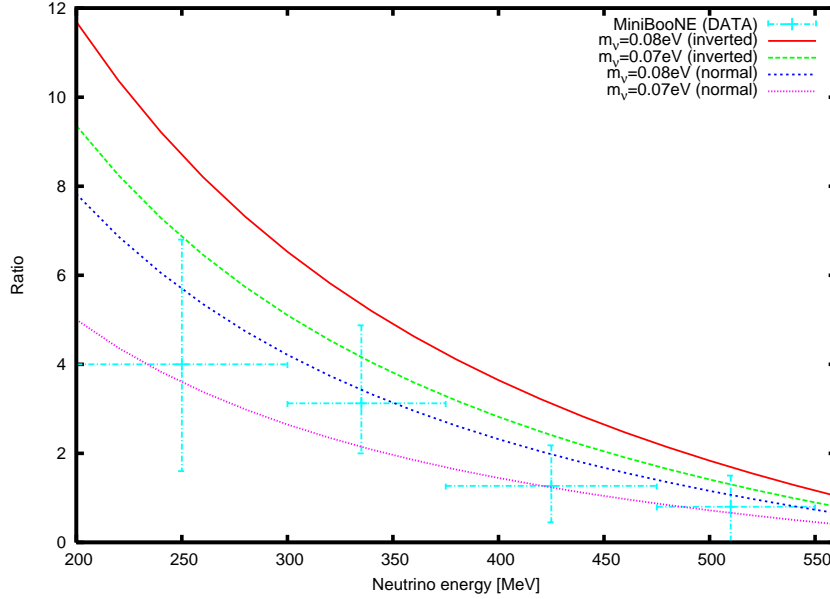


FIG. 8. (Color online) $P_{\nu_e}^{(d)}/P_{\nu_e}^{(0)}(\mu)$ is compared with MiniBooNE data (light-blue) including statistic and systematic errors [18]. For numerical calculation, $m_{\nu_h} = 0.07$ eV (green: inverted, magenta: normal), $m_{\nu_h} = 0.08$ eV (red: inverted, blue: normal), $E_\mu = 670$ MeV, and $E_\pi = 1.15$ GeV are used.

Figure 9 shows energy dependence of ratio $P_{\nu_e}^{(d)}/P_{\nu_e}^{(0)}$ of our theory at MicroBooNE experiment [19]. In this experiment, the neutrino beam is the same as that of MiniBooNE. MicroBooNE detector is smaller than that of MiniBooNE but the target nucleus is ^{40}Ar , whose size is much larger than ^{12}C and the finite-size correction also becomes large. With using two different lengths of decay region and sufficient statistics, not only the absolute neutrino mass but also the mass hierarchy can be determined.

B. Neutrino flavor changes through diffraction in μ^+ decay

The diffraction causes a flavor change at short-distance which is different from the ordinary flavor oscillation. In $\mu^+\text{DAR}$,

$$\mu^+ \rightarrow e^+ + \bar{\nu}_\mu + \nu_e, \quad (110)$$

$\bar{\nu}_e$ does not exist in this process. However, there are several processes that $\bar{\nu}_e$ is detected at near-detectors of $L \sim 10 - 100$ m in μ^+ decay. One is a flavor oscillation with a large Δm^2 of the order of 1 eV^2 or less, and another is from finite-size corrections to the probability

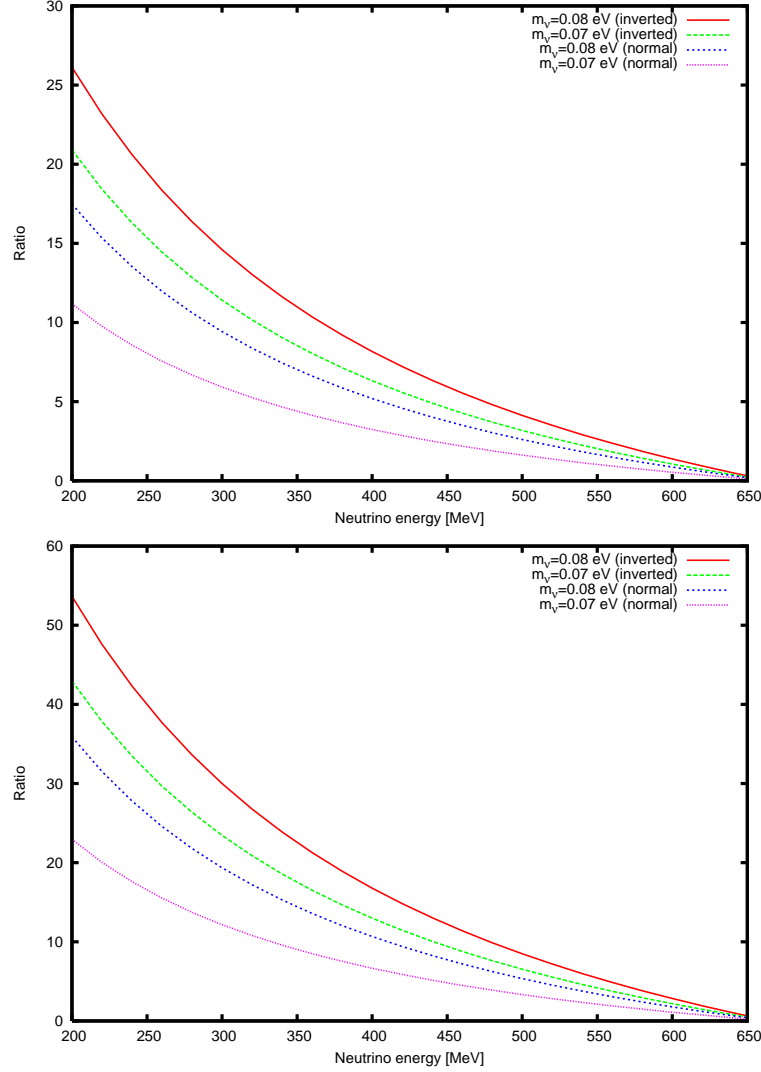


FIG. 9. (Color online) Energy dependences of the ratio $P_{\nu_e}^{(d)} / P_{\nu_e}^0$ of our theory for MicroBooNE [19] setup are shown. Top figure is of $cT = 50$ m and bottom one is of 25 m. For numerical calculation, $m_{\nu_h} = 0.07$ eV (green: inverted, magenta: normal), $m_{\nu_h} = 0.08$ eV (red: inverted, green: normal), $E_\mu = 670$ MeV, and $E_\pi = 1.15$ GeV are used. Target nucleus is ^{40}Ar .

to detect a neutrino at finite T . The former requires at least one new kind of neutrino that does not have electro-magnetic or weak interaction, so-called sterile neutrino [16, 17], but the latter does not. $\bar{\nu}_e$ appears through the flavor change effect of finite-size correction even without sterile neutrinos, we study its magnitude and spectrum in this section. Since it has different energy spectra with that of flavor oscillation, it is possible to distinguish experimentally.

In μ^+ DIF, both ν_μ appearance and $\bar{\nu}_\mu$ disappearance can be observed in charged current

interactions because neutrinos have high energies enough to create muons. Since finite-size corrections are positive definite, not only $\bar{\nu}_\mu$ but also ν_μ has an excess in its flux. In order to distinguish the finite-size correction from the neutrino oscillation with sterile neutrino clearly, μ^+ DIF experiments are desirable.

1. LSND and KARMEN (μ^+ DAR)

There are two experiments of similar geometry that use μ^+ DAR to search the $\bar{\nu}_e$ appearance at near-detectors. One is LSND [20] and the other is KARMEN [21]. LSND reported the event excess that is explained by flavor oscillation with $(\Delta m_{LSND}^2, \sin^2 2\theta_{LSND}) = (1.2\text{eV}^2, 0.003)$ as the best-fit, whereas no excess was observed in KARMEN. They are not consistent each other under a sterile-neutrino-flavor-oscillation hypothesis. Comparisons of parameters and results of two experiments are summarized in Table I. The geometry of the μ^+ DAR experiment is shown in Fig. 10. The important difference between them in our analyses is the time difference denoted as Δt . Δt is time difference between the prompt signal from positron in anti-beta decay and delayed signal from neutron capture. KARMEN required the time difference of delayed coincidence of $5 < \Delta t < 300\mu\text{s}$ but LSND used likelihood-ratio instead of Δt . This makes essential difference in our theoretical calculation. We examine about it later in this section. We compute the effects of the flavor change thorough the finite-size correction under experimental conditions of LSND and KARMEN and compare the spectrum of the correction with that of flavor oscillation with sterile neutrino. We show that the corrections are different and consistent with experiments.

The energy spectra from the finite-size correction and flavor oscillation caused by fourth neutrino are given by

$$\frac{dP^{(d)}}{dE_{\bar{\nu}_e}} = \frac{G_F^2 m_\mu^2 \tau_\mu}{12\pi^3} E_{\bar{\nu}_e}^2 \frac{m_\mu^2 \sigma_{\bar{\nu}_e}}{8\pi} \left(1 - 2\frac{E_{\bar{\nu}_e}}{m_\mu}\right) \left(5 - 6\frac{E_{\bar{\nu}_e}}{m_\mu}\right) \tilde{g}_{\mu,e}(\omega_{\bar{\nu}_e}, T; \tau_\mu), \quad (111)$$

$$\frac{dP^{\text{osc}}}{dE_{\bar{\nu}_e}} = \frac{G_F^2 m_\mu^2 \tau_\mu}{12\pi^3} E_{\bar{\nu}_e}^2 \left(3 - 4\frac{E_{\bar{\nu}_e}}{m_\mu}\right) \left(e^{-\frac{T_\mu}{\tau_\mu}} - e^{-\frac{(T_\mu + T_D)}{\tau_\mu}}\right) \sin^2 2\theta \sin\left(1.27 \frac{\Delta m^2}{E_\nu} L\right). \quad (112)$$

The former has no free parameter, but the latter has new mass-squared difference δm^2 . The ratio $\frac{dP^{(d)}/dE}{dP^{\text{osc}}/dE}$ of LSND and KARMEN are shown in Fig. 11. The parameters shown in Table I are used to calculate the ratios numerically. From this figure, $P^{(d)}$ for LSND parameters

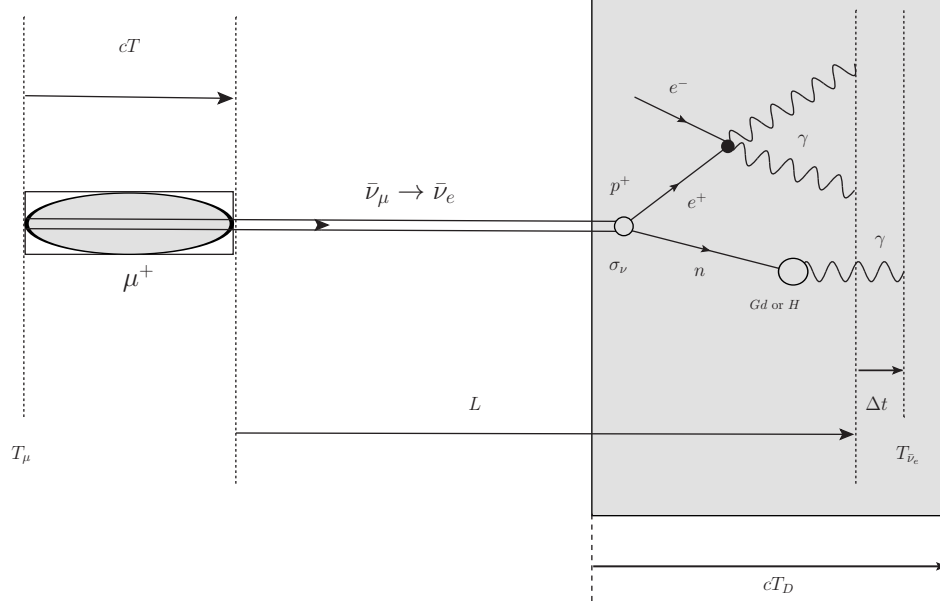


FIG. 10. Time structure of the detection of $\bar{\nu}_e$ through anti beta decay with the delayed coincidence in μ^+ DAR is shown. T is the time width where μ^+ and decay products can overlap. L is length between the decay region and the detector that is used in flavor oscillation formula. Δt is time difference between the photon signals of positron and neutron capture that is used for event selection in KARMEN experiment.

is in the same order of the magnitude with flavor oscillation with LSND best-fit parameters while that for KARMEN vanishes. This difference results from methods of event selection they used.

The diffraction term has its origin in overlap of wave functions of parent and daughters. The non-stationary nature is caused by this property, and structure in time is very different from that of normal component of stationary state. Following Fig. 10, the detector is located away from the muon decay region and the time region of the overlap is defined as $T = T_{\bar{\nu}_e} - T_\mu - L/c$ for μ^+ DAR geometry. If the time difference between photons from positron and those from neutron, Δt , is not used for event selection, the overlapping region T is the size of beam stop and the diffraction term is automatically included into the event of $\bar{\nu}_e$. However, when the time difference is used, the overlapping region is modified by Δt as $T = T_{\bar{\nu}_e} - T_\mu - L/c - \Delta t$. Then, only in case of $T > 0$, the events include the diffraction term.

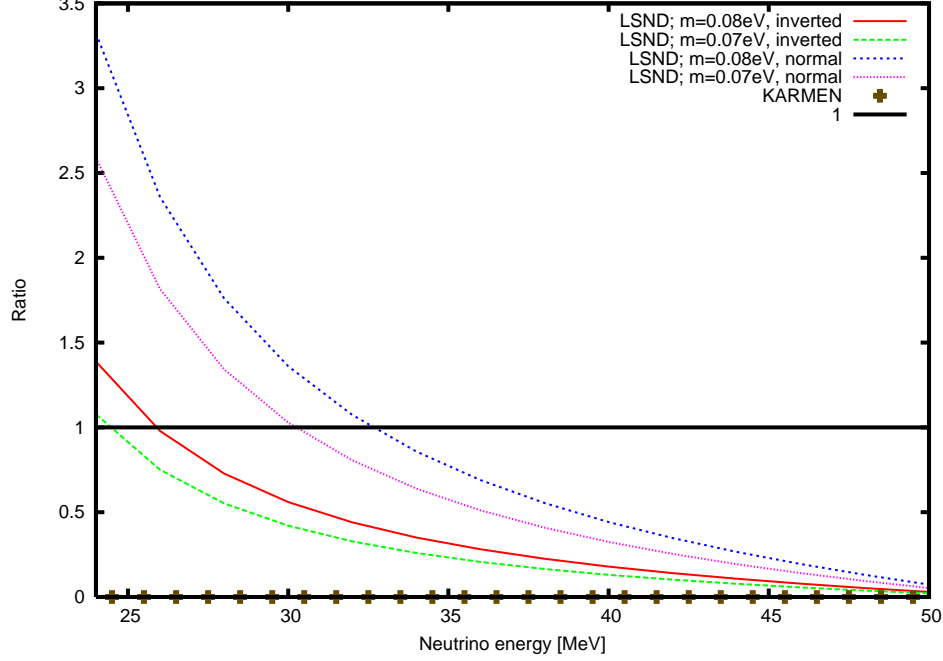


FIG. 11. (Color online) The ratios $\frac{dP^{(d)}/dE}{dP^{osc}/dE}$ are shown. For LSND, $T_\mu = 0$, $cT = 0.8\text{m}$ ($T \sim 2.5\text{ns}$), $cT_D = 8.3\text{ m}$, $L = 29.8\text{m}$, $\sigma_{\bar{\nu}_e}^{\text{LSND}}$ of $C_{2n}H_{2n+2}$, $\Delta m_{LSND}^2 = 1.2\text{eV}^2$, and $\sin^2 2\theta_{LSND} = 0.003$ are used. Red curve shows inverted hierarchy of $m_{\nu_h} = 0.08\text{ eV}$, green curve shows inverted of $m_{\nu_h} = 0.07\text{ eV}$, blue curve shows normal hierarchy of $m_{\nu_h} = 0.08\text{ eV}$, and magenta curve shows normal of $m_{\nu_h} = 0.07\text{ eV}$. For KARMEN, $T_\mu = 0.3\mu\text{s}$, $\Delta t = 5\mu\text{s}$, $cT = 0.3\text{m}$ ($T \sim 1.0\text{ns}$), $cT_D = 3.5\text{ m}$, $m_{\nu_h} = 0.08\text{ eV}$ of inverted hierarchy, $L = 17.7\text{m}$, angle between proton beam and detector $\theta = 100^\circ$, $\sigma_{\bar{\nu}_e}^{\text{KARMEN}}$, $\Delta m_{LSND}^2 = 1.2\text{eV}^2$ and $\sin^2 2\theta_{LSND} = 0.003$ are used. A geometry for $\mu^+\text{DAR}$ is shown in Fig. 10 and a relation between T and θ is given in Appendix C 4.

KARMEN used Δt for event selection as $\Delta t > 5\mu\text{s}$ whereas LSND did not. Consequently the diffraction is included in LSND but not in KARMEN. This difference in both event selections naturally explains the disagreement between those two experiments that seems to be difficult to interpret as flavor oscillation. In addition, if the events for $\Delta t < T$ are included, $\bar{\nu}_e$ excess must be seen in KARMEN. Δt dependence of ratio are given in Fig. 12. The magnitude of $P^{(d)}$ is almost the same magnitude with that of LSND. An indication may appear as a sharp peak in small Δt region in Ref. [21].

According to above analyses, both two experimental results of LSND and KARMEN can be explained with the finite-size corrections, and are consistent with the previous result of LSND πDIF [15]. Furthermore, with more precise energy spectrum and suitable selection

	LSND	KARMEN
Size of beam stop (D×W×H)	1m×0.2m×0.2m	0.5m× 0.25m×0.25m
L	29.8m	17.7m
Δt	No	$5\mu s < \Delta t < 300\mu s$
Scintillator	CH_2	$C_n H_{2n+2}(75\%) + C_9 H_{12}(25\%)$
$E_{\bar{\nu}_e}$	36(20)–60MeV	16–50MeV
Primary positron time window	No, $T_\mu = 0$	$0.6\mu s < T_\mu < 10\mu s$
T_D , Depth of detector	8.3 m	3.5 m
Detector angle	10°	100°
$\bar{\nu}_e$ event excess	$87.9 \pm 22.4 \pm 6.0$	No excess
Best fit Δm^2 and $\sin^2 \theta$	$\Delta m^2 = 1.2 \text{ eV}^2$, $\sin^2 \theta = 0.003$	None

TABLE I. Parameters and results of LSND and KARMEN.

criteria, it is possible to confirm the excess of $\bar{\nu}_e$ at near-detector as diffraction.

2. Future experiments of μ^+ DAR and μ^+ DIF

There are two possible experiments to confirm the excess of flux of neutrino from μ^+ decay as the finite-size correction. One is a $\bar{\nu}_e$ appearance experiment with μ^+ DAR [23]. The other is a ν_μ appearance and $\bar{\nu}_\mu$ disappearance with μ^+ DIF [24]. Here, we give predictions for future experiments of both cases.

1. μ^+ DAR

In μ^+ DAR experiments, $\bar{\nu}_e$ spectrum is given by Eq. (111). Without requiring the double coincidence condition of Δt , the ratio between $\bar{\nu}_e$ and $\bar{\nu}_\mu$ spectra is written as

$$R_{\bar{\nu}_e}(E_\nu) = \frac{m_\mu^2 \sigma_{\bar{\nu}_e}}{8\pi} \frac{\left(1 - 2\frac{E_\nu}{m_\mu}\right) \left(5 - 6\frac{E_\nu}{m_\mu}\right)}{\left(3 - 4\frac{E_\nu}{m_\mu}\right) \left(e^{-\frac{T_\mu}{\tau_\mu}} - e^{-\frac{T_\mu + T_D}{\tau_\mu}}\right)} \tilde{g}_{\mu,e}(\omega_{\bar{\nu}_e}, T; \tau_\mu). \quad (113)$$

This is the simplest value under ideal conditions. The value for an experimental setup [23] is shown in Fig. 13, where cT , the size of beam stop, is 1 m, $T_\mu = 1 \mu s$, $cT_D = 3.4$ m, and $\sigma_{\bar{\nu}_e}$ is of $C_{2n}H_{2n+2}$ in the liquid scintillator. The magnitude compared with the expected $\bar{\nu}_e$ appearance by the simple flavor oscillation with one sterile neutrino is found in the ratio,

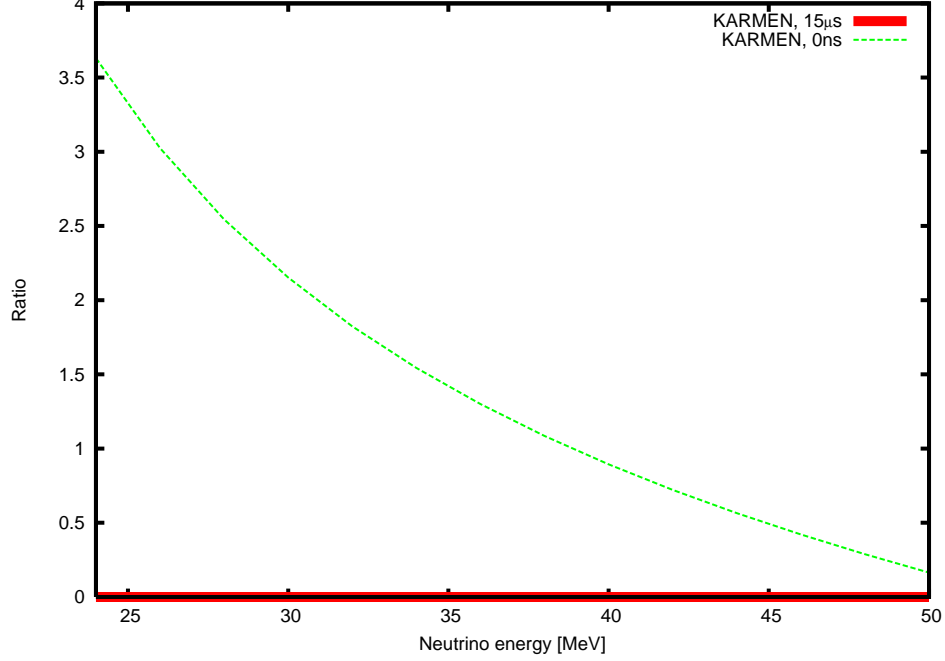


FIG. 12. (Color online) Δt dependence of ratio for KARMEN. $\Delta t = 0$ ns (green), and $\Delta t = 5\mu s$ (red). We use $m_{\nu_h} = 0.08$ eV of inverted hierarchy and all other parameters are same with Fig. 11.

$$\frac{dP^d/dE}{dP^{\text{osc}}/dE},$$

$$R_{\bar{\nu}_e}^{\text{osc}}(E_\nu) = \frac{m_\mu^2 \sigma_{\bar{\nu}_e}}{8\pi} \frac{\left(1 - 2\frac{E_\nu}{m_\mu}\right) \left(5 - 6\frac{E_\nu}{m_\mu}\right) \tilde{g}_{\mu,e}(\omega_{\bar{\nu}_e}, T; \tau_\mu)}{\left(3 - 4\frac{E_\nu}{m_\mu}\right) \left(e^{-\frac{T_\mu}{\tau_\mu}} - e^{-\frac{T_\mu + T_D}{\tau_\mu}}\right) \sin^2 2\theta_{\mu e} \sin^2 \left(1.27 \frac{\Delta m_{41}^2 L}{E_\nu}\right)}. \quad (114)$$

Figure 14 shows the ratio Eq. (114), where experimental parameters are same with Fig. (13) and parameters of sterile neutrino are [17]

$$U_{e4} = 0.15, \quad U_{\mu 4} = 0.17, \quad (115)$$

$$\sin^2 \theta_{\mu e} = 4 |U_{\mu 4} U_{e4}|^2, \quad (116)$$

$$\sin^2 \theta_{\mu \mu} = 4 |U_{\mu 4}|^2 (1 - |U_{\mu 4}|^2), \quad (117)$$

$$\Delta m_{41}^2 = 0.9 \text{ eV}^2. \quad (118)$$

These values are also used in next μ^+ DIF case. According to Figs. 13 and 14, the magnitude of $\bar{\nu}_e$ appearance through the finite-size correction can be almost same with or larger than that of the flavor oscillation with the sterile neutrinos. Furthermore, the effect is sensitive to the absolute neutrino mass and the mass hierarchy of neutrino.

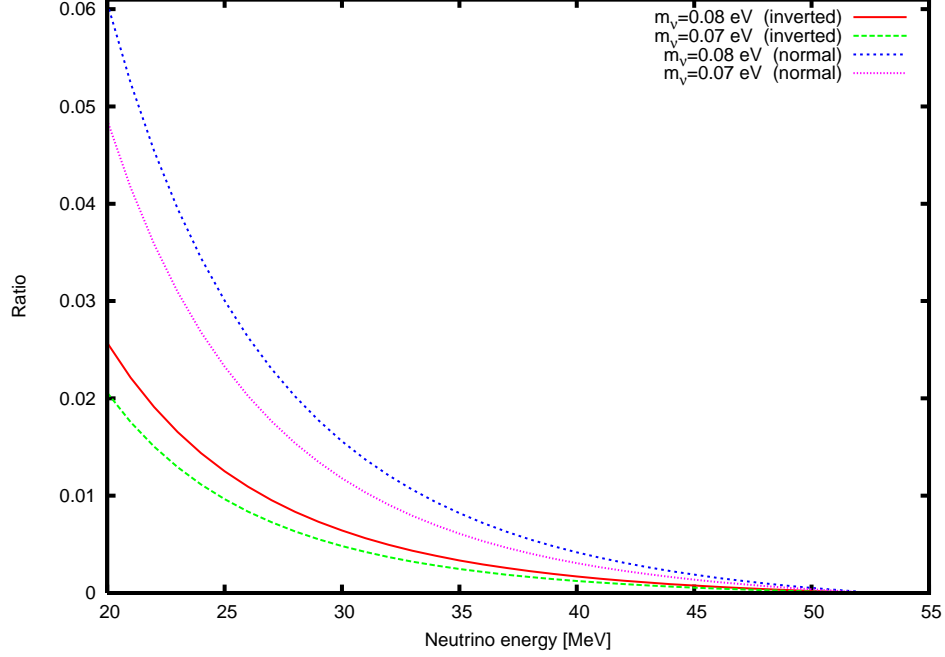


FIG. 13. (Color online) The ratios $\frac{dP_{\bar{\nu}_e}^{(d)}/dE}{dP_{\bar{\nu}_\mu}^{(d)}/dE}$, Eq. (113), for μ^+ DAR are shown, where $T_\mu = 1 \mu\text{s}$, $cT = 1.0 \text{ m}$, $L = 17.0\text{m}$, and $\sigma_{\bar{\nu}_e} = 7.3$ of $C_{2n}H_{2n+2}$ and $cT_D = 3.4 \text{ m}$ are used [23]. Red curve shows inverted hierarchy of $m_{\nu_h} = 0.08 \text{ eV}$, green curve shows inverted of $m_{\nu_h} = 0.07 \text{ eV}$, blue curve shows normal hierarchy of $m_{\nu_h} = 0.08 \text{ eV}$, and magenta curve shows normal of $m_{\nu_h} = 0.07 \text{ eV}$.

2. μ^+ DIF

In μ^+ DIF experiment, an appearance of ν_μ ($\nu_e \rightarrow \nu_\mu$) from ν_e and a disappearance of $\bar{\nu}_\mu$ ($\bar{\nu}_\mu \rightarrow \bar{\nu}_e$) will be searched since the flavor oscillation with sterile neutrinos are kept in mind. However, the finite-size corrections provide appearance of ν_μ and $\bar{\nu}_\mu$, and their magnitude and spectra are very different from those of sterile neutrinos. Using Eqs. (101) – (104), the ratios $\frac{P_{\nu_\mu}^{(d)}(E_\nu)}{P_{\nu_\mu}^{osc}(E_\nu)}$ and $\frac{P_{\bar{\nu}_\mu}^{(d)}(E_\nu)}{P_{\bar{\nu}_\mu}^{osc}(E_\nu)}$ are written as

$$R_{\nu_\mu}(E_\nu, \cos \theta) = \frac{\sigma_{\nu_\mu}(m_\mu^2 - 2E_\nu(E_\mu - p_\mu \cos \theta))\tilde{g}_{e,\mu}(\omega_\nu, T; \gamma\tau_\mu)}{2\pi \left(\exp \left[-\frac{T_\mu}{\gamma\tau_\mu} \right] - \exp \left[-\frac{T_\mu+T}{\gamma\tau_\mu} \right] \right) \sin^2 2\theta_{\mu e} \sin^2 \left(1.27 \frac{\Delta m_{41}^2}{E_\nu} L \right)}, \quad (119)$$

$$R_{\bar{\nu}_\mu}(E_\nu, \cos \theta) = \frac{\sigma_{\bar{\nu}_\mu}(m_\mu^2 - 2E_\nu(E_\mu - p_\mu \cos \theta))\tilde{g}_{e,\mu}(\omega_\nu, T; \gamma\tau_\mu)}{2\pi \left(\exp \left[-\frac{T_\mu}{\gamma\tau_\mu} \right] - \exp \left[-\frac{T_\mu+T}{\gamma\tau_\mu} \right] \right) \left(1 - \sin^2 2\theta_{\mu\mu} \sin^2 \left(1.27 \frac{\Delta m_{41}^2}{E_\nu} L \right) \right)}, \quad (120)$$

and that of $\bar{\nu}_\mu$ is given by Eq. (106). Eqs. (105) and (106) are given in Figs. 15 and 16. The target nucleus is ^{56}Fe and parameters given in Eqs. (115)–(118) are used. The ratio of ν_μ

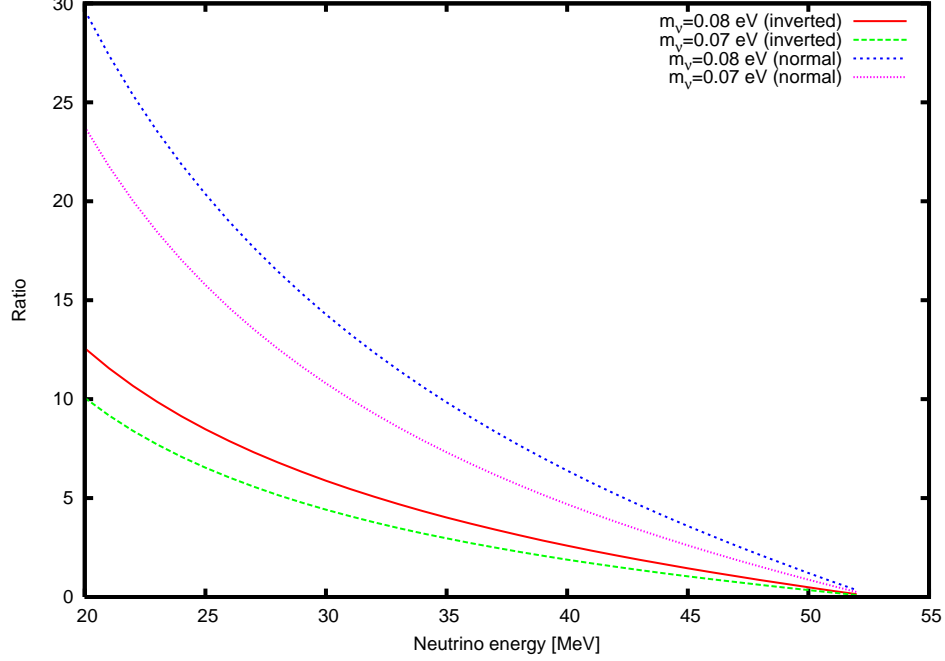


FIG. 14. (Color online) The ratios $\frac{dP_{\nu_e}^{(d)}/dE}{dP_{\nu_e}^{osc}/dE}$, Eq. (114), for μ^+ DAR are shown, where $T_\mu = 1 \mu s$, $cT = 1.0 \text{ m}$, $L = 17.0 \text{ m}$, $cT_D = 3.4 \text{ m}$, and $\sigma_{\bar{\nu}_e} = 7.3$ of $C_{2n}H_{2n+2}$ and are used [23]. Red curve shows the ratio of the inverted hierarchy with $m_{\nu_h} = 0.08 \text{ eV}$, green curve shows that of the inverted hierarchy with $m_{\nu_h} = 0.07 \text{ eV}$, blue curve shows the ratio of the normal hierarchy with $m_{\nu_h} = 0.08 \text{ eV}$, and magenta curve shows the ratio of the normal hierarchy with $m_{\nu_h} = 0.07 \text{ eV}$.

appearance at $L = 20 \text{ m}$ is very large. This is because T dependences are different in normal and diffraction terms. The normal term is very small at $T \ll \gamma\tau_\mu$ and P^0 increases with T , but the diffraction term $P^{(d)}$ is constant in T . In addition, the oscillation length with $\Delta m_{41}^2 = 0.9 \text{ eV}^2$ at $E_\nu = 1 \text{ GeV}$ is 800–900 m and the effect of the flavor oscillation is not significant at $L = 20 \text{ m}$. Then, 10^3 larger magnitude of ν_μ appearance through the finite-size correction at $L = 20 \text{ m}$ is a natural consequence with the nature of diffraction term. Then, the relative magnitude between them becomes very large of order 10^3 at $cT = 226 \text{ m} \ll \gamma\tau_\mu$ of $E_\mu = 3 \text{ GeV}$.

The ratio of ν_μ appearance at $L = 2000 \text{ m}$ has three peaks because the numerator $dP_{\nu_\mu}^{(d)}/dE_\nu$ varies uniformly in energy and the denominator $dP_{\nu_\mu}^{osc}/dE_\nu$ oscillates in energy and becomes very small at certain energies.

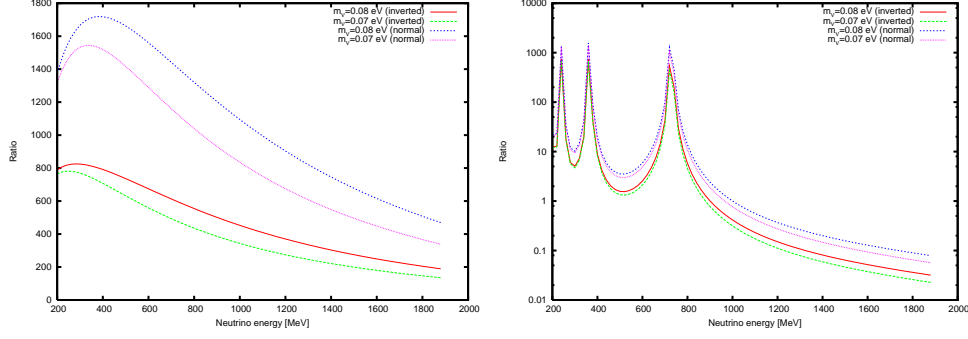


FIG. 15. (Color online) The ratios of ν_μ appearance $\frac{dP_{\nu_\mu}^{(d)}/dE_\nu}{dP_{\nu_\mu}^{osc}/dE_\nu}$, Eq. (114), for μ^+ DIF are shown, where $T_\mu = 0 \mu s$, $cT = 226.0$ m, $L = 20.0$ m (Left) and $L = 2000.0$ m (Right), and σ_{ν_μ} = of ^{56}Fe and $\cos \theta = 1$ are used [24]. Red curve shows the ratio of the inverted hierarchy with $m_{\nu_h} = 0.08$ eV, green curve shows that of the inverted hierarchy with $m_{\nu_h} = 0.07$ eV, blue curve shows the ratio of the normal hierarchy with $m_{\nu_h} = 0.08$ eV, and magenta curve shows the ratio of the normal hierarchy with $m_{\nu_h} = 0.07$ eV. In the right figure, there are three sharp peaks because the denominator oscillates in energy and becomes very small.

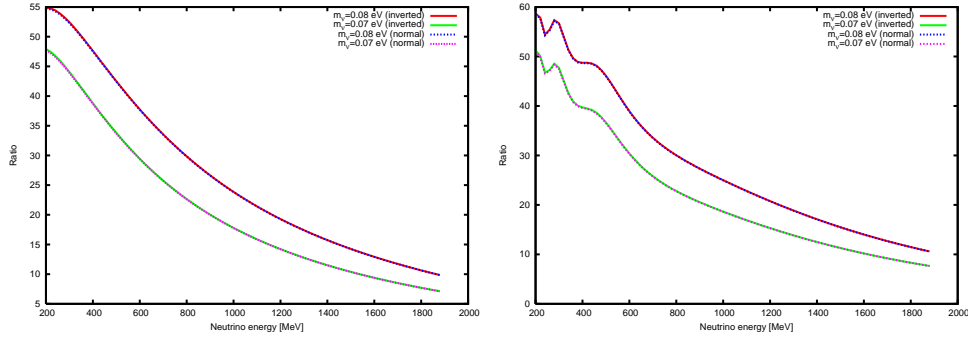


FIG. 16. (Color online) The ratios of excess and disappearance of $\bar{\nu}_\mu$, $\frac{dP_{\bar{\nu}_\mu}^{(d)}/dE}{dP_{\bar{\nu}_\mu}^{osc}/dE}$, Eq. (114), for μ^+ DIF are shown, where $T_\mu = 0 \mu s$, $cT = 226.0$ m, $L = 20$ m (Left) and $L = 2000$ m (Right), and $\sigma_{\bar{\nu}_\mu}$ = of ^{56}Fe and $\cos \theta = 1$ are used [24]. Red curve shows the ratio of the inverted hierarchy with $m_{\nu_h} = 0.08$ eV, green curve shows that of the inverted hierarchy with $m_{\nu_h} = 0.07$ eV, blue curve shows the ratio of the normal hierarchy with $m_{\nu_h} = 0.08$ eV, and magenta curve shows the ratio of the normal hierarchy with $m_{\nu_h} = 0.07$ eV.

V. THE ELECTRON SPECTRUM

Next, we study the finite-size corrections to the probability to detect the electron. Two un-observed neutrinos are expressed with plane waves and their momenta are integrated.

A. Asymptotic value

The spectrum of the electron at $T \rightarrow \infty$ is

$$\frac{d\Gamma^0}{dx} = \frac{G_F^2 m_\mu^5}{96\pi^3} x^2 (3 - 2x), \quad x = \frac{2E_e}{m_\mu}, \quad (121)$$

for μ DAR. The electron mass and radiative corrections are neglected here.

B. Probability

The total probability of the event that the electron is detected is expressed in the form,

$$P_e = \left(\frac{\pi^2}{\sigma_\mu \sigma_e} \right)^{\frac{3}{2}} \frac{G_F^2 2^8}{E_\mu (2\pi)^3} \int \frac{d\vec{X}_e d\vec{p}_e d\vec{p}_{\nu_e} d\vec{p}_{\nu_\mu}}{E_e E_{\nu_e} E_{\nu_\mu} (2\pi)^{12}} (p_\mu \cdot p_{\nu_e})(p_e \cdot p_{\nu_\mu}) |I(\delta p)|^2, \quad (122)$$

$$I(\delta p) = \int d^4 x e^{-i\delta\phi(x)} e^{-\frac{t}{2\tau_\mu}} w(x, X_\mu; \sigma_\mu) w(x, X_e; \sigma_e).$$

The probability, Eq. (122) is written in the form,

$$P_e = N \int d\vec{X}_e \frac{d\vec{p}_e}{E_e} \frac{d\vec{p}_{\nu_e}}{E_{\nu_e}} \frac{d\vec{p}_{\nu_\mu}}{E_{\nu_\mu}} \frac{1}{2} \sum_{spin} |\mathcal{M}|^2$$

$$= N' \int d\vec{X}_e \frac{d\vec{p}_e}{E_e} d^4 x_1 d^4 x_2 e^{ip_e \cdot \delta x} e^{-\frac{t_1+t_2}{2\tau_\mu}} \Delta_{\nu_e, \nu_\mu}(\delta x)$$

$$\times w(x_1, X_\mu; \sigma_\mu) w(x_2, X_\mu; \sigma_\mu) w(x_1, X_e; \sigma_e) w(x_2, X_e; \sigma_e), \quad (123)$$

where the correlation function $\Delta_{\nu_e, \nu_\mu}(\delta x)$ is defined as

$$\Delta_{\nu_e, \nu_\mu}(\delta x) = \frac{1}{(2\pi)^6} \int \frac{d\vec{p}_{\nu_e} d\vec{p}_{\nu_\mu}}{E_{\nu_e} E_{\nu_\mu}} (p_\mu \cdot p_{\nu_e})(p_e \cdot p_{\nu_\mu}) e^{i(p_{\nu_e} + p_{\nu_\mu} - p_\mu) \cdot \delta x}, \quad (124)$$

and details are given in Appendix B 3 b. From Eq. (B21) and integration by parts, the probability is written in the form

$$P_e = P_e^0 + P_e^{(light-cone)} + P^{(regular)}$$

$$= N' \int d\vec{X}_e \frac{d\vec{p}_e}{E_e} \int d^4 x_1 d^4 x_2 e^{ip_e \cdot \delta x} e^{-\frac{t_1+t_2}{2\tau_\mu}} \prod_{1,2} w(x_i, X_\mu; \sigma_\mu) w(x_i, X_e; \sigma_e)$$

$$\times \frac{1}{12(2\pi)^2} \int^{m_\mu^2 - 2p_\mu \cdot p_e} dm^2 \rho(m^2) \left[\text{“Normal term”} + i \frac{\epsilon(\delta t)}{4\pi} \delta(\lambda) + J_{\text{regular}} \right], \quad (125)$$

$$\rho(m^2) = (p_\mu \cdot p_e) m^2 + 2(m_\mu^2 - p_\mu \cdot p_e)(p_\mu \cdot p_e - m_e^2).$$

For large $\sigma_\mu (\approx \infty)$, the most singular part is

$$\begin{aligned}
P_e^{(light-cone)} &= \frac{N'}{12(2\pi)^2} \int \frac{d\vec{p}_e}{E_e} \int^{m_\mu^2 - 2p_\mu \cdot p_e} dm^2 \rho(m^2) \int d^4x_1 d^4x_2 \prod_{1,2} w(x_i, X_\mu; \sigma_\mu) w(x_i, X_e; \sigma_e) \\
&\quad \times i \frac{\epsilon(\delta t)}{4\pi} \delta(\lambda) e^{ip_e \cdot \delta x} e^{-\frac{t_1+t_2}{2\tau_\mu}} \\
&\simeq \frac{N'}{12(2\pi)^2} \int \frac{d\vec{p}_e}{E_e} \int^{m_\mu^2 - 2p_\mu \cdot p_e} dm^2 \rho(m^2) \frac{i\sigma_e}{2} \int dt_1 dt_2 \frac{e^{i\omega_e \delta t}}{\delta t} e^{-\frac{(1-|\vec{v}_e|)^2 \delta t^2}{4\sigma_e}} e^{-\frac{t_1+t_2}{2\tau_\mu}},
\end{aligned} \tag{126}$$

where $\delta t = t_1 - t_2$ and $\omega_e = \frac{m_e^2}{2E_e}$. In Eq. (126), $1 - |\vec{v}_e|$ in the exponent cannot be ignored because the mass of electron is much larger than that of neutrino; $e^{-\frac{(1-|\vec{v}_e|)^2 \delta t^2}{4\sigma_e}}$ factor represents a loss of overlap of wave functions and makes $P_e^{(light-cone)}$ short range. $P^{(regular)}$ also has this suppression factor. So the correction exists only at $T \lesssim T_d = \frac{2\sqrt{\sigma_e}}{1-|\vec{v}_e|}$. The high-energy electron is measured with bremsstrahlung and the scale of this process is around 10^{-13} m. So we use this value for σ_e . For $\sqrt{\sigma_e} \sim 10^{-13}$ m, $T_0 = 1/\omega_e$ and T_d for various electron energies are summarized in Table II.

E_e	$T_0 = 1/\omega_e$	T_d	ϵ_0
30 MeV	5×10^{-11} m	7×10^{-10} m	5×10^{-13}
300 MeV	5×10^{-10} m	7×10^{-8} m	10^{-11}
1 GeV	1.5×10^{-9} m	1.6×10^{-6} m	5×10^{-10}
8 TeV	1.3×10^{-5} m	1×10^2 m	3×10^{-4}
1 PeV	1.3×10^{-2} m	$> 1 \times 10^8$ m	10^2
1 GeV with $\sqrt{\sigma_e} = 10^{-8}$ m	1.5×10^{-9} m	1.6×10^{-1} m	7×10^{-3}

TABLE II. T_0 , T_d , and ϵ_0 for various electron energies.

T_d became macroscopic for neutrino but becomes microscopic for electron except for high-energy regions or large σ_e . Due to these properties, only the upper bound of $P_e^{(light-cone)}$ can be obtained. The bound for the universal function $g(\omega_e, T; \tau_\mu)$ is given as

$$\begin{aligned}
&\int_0^T dt \frac{\sin \omega_e t}{t} \left(e^{-\frac{t}{2\gamma\tau_\mu}} - e^{-\frac{T}{\gamma\tau_\mu}} e^{\frac{t}{2\gamma\tau_\mu}} \right) e^{-\frac{(1-|\vec{v}_e|)^2}{4\sigma_e} \delta t^2} \leq \epsilon_0, \\
\epsilon_0 &= \sqrt{\pi \omega_e \gamma \tau_\mu \times \frac{T_d^3}{3\gamma^3 \tau_\mu^3}}.
\end{aligned} \tag{127}$$

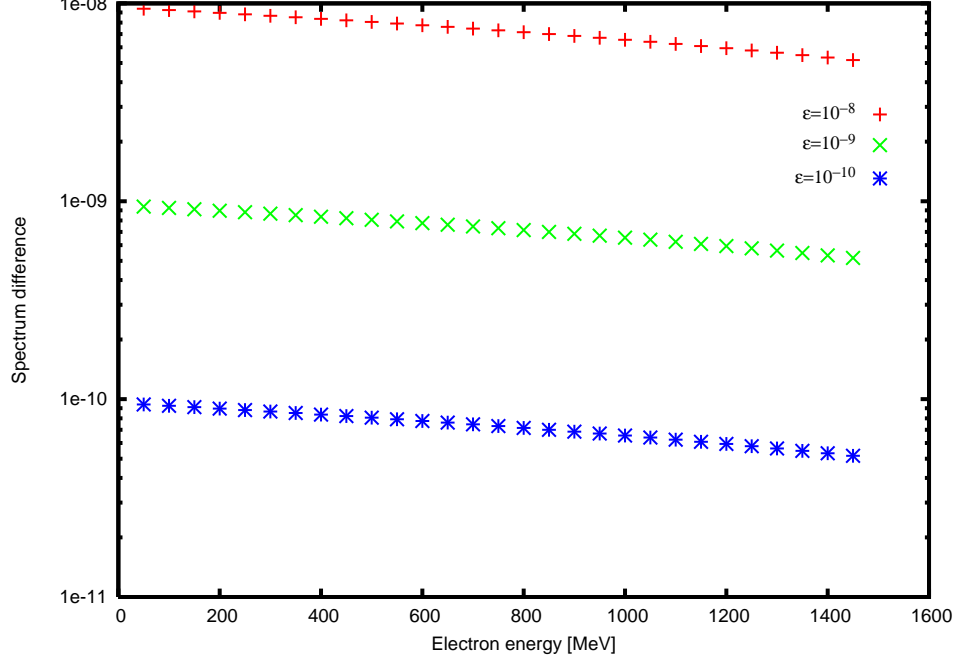


FIG. 17. (Color online) Spectrum differences of Eq. (133) for various ϵ are shown. Red, Green, and Blue curves correspond to $\epsilon = 10^{-8}$, 10^{-9} , and 10^{-10} , respectively. $\cos \theta = 1$.

For the electron of $E_e = 1$ GeV, the upper limit is

$$\epsilon_0 \sim 10^{-9}, \quad (128)$$

and the limits for other energy values are also given in Table II. By using Eq. (127), we have

$$\begin{aligned} \frac{d^2 P_e^{(light-cone)}}{dE_e d\cos\theta} &\leq \frac{G_F^2}{24\pi^3 E_\mu} \frac{E_e^2}{4\pi} (E_\mu - p_\mu \cos\theta)(m_\mu^2 - 2E_e(E_\mu - p_\mu \cos\theta)) \\ &\quad \times (5m_\mu^2 - 6E_e(E_\mu - p_\mu \cos\theta)) \gamma \tau_\mu \sigma_e \epsilon_0, \end{aligned} \quad (129)$$

$$\equiv \epsilon_0 \times \rho^{(d)}(E_e, \cos\theta). \quad (130)$$

The upper limit ϵ_0 is constant in T . According to the nature that the finite-size correction vanishes at $T \rightarrow \infty$, it is reasonable to assume the upper limit of the magnitude of $P_e^{light-cone} + P_e^{regular}$ to be $\epsilon_0 \rho^{(d)}(E_e)$. Compared with the previous neutrino case, the wave packet size $\sigma_e = 100 \times \sigma_{\bar{\nu}_\mu}$. Since the diffraction term is proportional to the wave packet size σ of detected particle, the diffraction term of electron is expressed as

$$\epsilon_0 \rho^{(d)}(E_e, \cos\theta) \sim 10^{-7} \times \rho_{\bar{\nu}_\mu}^{(d)}(E_{\bar{\nu}_\mu}, \cos\theta). \quad (131)$$

Because the ratio of normal and diffraction terms for $\bar{\nu}_\mu$ is of order 1, $P^{(light-cone)}$ could give the correction of order 10^{-7} at most in the experiments of $E_e \lesssim 1$ GeV. Although this value is larger than the present limit of precision of muon g-2 experiment [5], this is the maximum value and the true value would be smaller than 10^{-7} . Then, the electron spectrum is distorted as

$$\frac{d^2 P_e}{dE_e d\cos\theta} = \frac{d^2 P_e^0}{dE_e d\cos\theta} + \epsilon \rho^{(d)}(E_e, \cos\theta), \quad \epsilon < 10^{-7}, \quad (132)$$

with an appropriate normalization. A spectrum difference defined as

$$\Delta(E_e, \cos\theta) \equiv \epsilon \frac{\rho^{(d)}(E_e, \cos\theta)}{d^2 P_e^0 / dE_e d\cos\theta} \quad (133)$$

could be measured in the accurate experiments. $\Delta(E_e)$ for several ϵ are shown in Fig. 17. $\Delta(E_e, \cos\theta)$ depends on E_e weakly and its variation is of order ϵ . So, the result suggests that the effect could be significant in precise experiments in case that ϵ is not small.

Since both T_d and T_0 become macroscopic at very high energy region, the finite-size correction is important even for the electron from muon decay at $E_e \gtrsim 100$ GeV. Similarly, when a detector that has large quantum coherence and provides large size of wave packets for detected particle is employed, T_d can become macroscopic even at low-energy region. Since the finite-size correction is proportional to σ_e , that can be large and could not be ignored in experiments of large σ_e or very high energy even if T_0 is microscopic.

VI. SUMMARY

In this paper, we studied $P^{(d)}$ for muon decay in $T \leq \tau_\mu$, using the S-matrix $S[T]$ that satisfies the boundary conditions at finite T . In this region, the wave function is the superposition of the parent and decay products, and has the finite-expectation value of interaction Hamiltonian. Since total energy is conserved, kinetic energy is not constant and varies with position, and the state retains wave nature. The non-uniform behavior appears and is probed with the final state expressed by the wave packets. Using wave packets [4, 10], the space-time positions and momenta of particles were treated simultaneously, and the position dependent probability was computed.

The waves in overlapping region of the initial and undetected states include those of ultraviolet region and due to the constructive interference peculiar to relativistic system, the

light-cone singularity, which is real and long range, appears. The phase factor ϕ_g of wave function of observed particle almost cancels on the light cone, and becomes the function of mass, energy, $\Delta\vec{x} = \vec{x} - \vec{X} = c\vec{n}\Delta t$ and $\Delta t = t - T$, in the form $\phi_g = E\Delta t - \vec{p} \cdot \Delta\vec{x} \simeq \frac{m^2}{2E}\Delta t$, where \vec{n} is the unit vector along \vec{p} . The light-cone singularity is inevitable consequence of relativistic invariance. The waves of large momenta have the speed of light and their phases in time and space are canceled at the light cone, and the waves are added constructively. The sum of these waves forms the singularity in two point correlation function, which is a manifestation of the diffraction.

The neutrino flux has an excess of almost same magnitude as the asymptotic value at macroscopic distance. This is larger than that of neutrino in pion decay because of the longer life-time of muon than that of pion and difference of kinematics. A new physical quantity is defined using the position dependence of the final states in the muon decay in the similar manner to the pion decay [1, 2]. Comparisons of the theoretical values with experiments of LSND, MiniBooNE, and KARMEN are made, and it was shown that the theoretical values with three neutrinos are in accord with experiments, if the finite-size corrections are included. Because the finite-size corrections are sensitive to the absolute neutrino masses, future precision experiments will be able to determine the values and mass hierarchy.

The electron or positron in muon decay also has finite-size corrections but because of its larger mass, the coherence length $L_c = cE_e/m_e^2$ is much smaller than that of neutrino. Even so, the corrections can be observed in precise measurements such as muon g-2 experiments.

It is worthwhile to clarify the reason why the finite-size correction is computable with the present amplitude of $S[T]$ but not with the normal scattering amplitude of $S[\infty]$. The normal scattering amplitude is defined between the in-state at $t = -\infty$ and out-state at $t = \infty$, and the space and time coordinates are integrated from $-\infty$ to ∞ so that the Poincare invariance is apparent and the energy and momentum of out-state is the same with those of in-state. Hence, the momentum of the electron in the final state is bounded. So the infinite momentum is not included in the final states and the light-cone singularity does not contribute to the transition amplitude and probability. The probability at the finite-time interval T , i.e., the non-asymptotic value, is not computable. In the amplitude of $S[T]$, the conservation law of kinetic energy and momentum does not hold and the infinite momentum states for the un-observed particle are included. They are necessary from the completeness to compute the correct probability. These states give the light-cone singularity of the correlation function

and the finite-size correction, which shows the excess of the neutrino flux or appears in spectra. They do not contribute to the asymptotic value, however. Hence, using the wave packet representation, the finite-distance behavior that is not capable of computing in the standard momentum representation was found.

In this paper, we studied a new quantum interference effect in the lowest order in G_F , since the effect is independent of higher-order corrections. The case in which the muon is described in small wave packet and other phenomena where the finite-size corrections play important roles will be presented in separate publication.

ACKNOWLEDGMENTS

This work was partially supported by a Grant-in-Aid for Scientific Research (Grant No. 24340043). Authors thank Dr. Kobayashi, Dr. Nishikawa, and Dr. Maruyama for useful discussions on the near-detector of T2K experiment, Dr. Asai, Dr. Kobayashi, Dr. Mori, and Dr. Yamada for useful discussions on interferences, Dr. Kinoshita and Dr. Nio for useful discussions on muon g-2 experiment.

Appendix A: Life-time effect on normal term

In $T \approx \tau_\mu$, the muon's life-time cannot be ignored and we have

$$\begin{aligned}
|I^{\text{normal}}(\delta p)|^2 &= \left(\frac{2\pi\sigma_\mu\sigma_{\nu_e}}{\sigma_\mu + \sigma_{\nu_e}} \right)^3 \exp \left[-\frac{\sigma_\mu\sigma_{\nu_e}}{(\sigma_\mu + \sigma_{\nu_e})} \delta \vec{p}^2 - \frac{(\tilde{X}_\mu - \tilde{X}_{\nu_e})^2}{(\sigma_\mu + \sigma_{\nu_e})} \right] \\
&\times \int dt_1 dt_2 e^{-\frac{t_1+t_2}{\tau_\mu} + i(\delta p^0 - \vec{v}_0 \cdot \delta \vec{p})(t_1 - t_2)} \\
&\times \exp \left[\frac{(\vec{v}_{\nu_e} - \vec{v}_\mu) \cdot (\tilde{X}_{\nu_e} - \tilde{X}_\mu)}{\sigma_\mu + \sigma_{\nu_e}} (t_1 + t_2) - \frac{(\vec{v}_{\nu_e} - \vec{v}_\mu)^2}{2(\sigma_\mu + \sigma_{\nu_e})} (t_1^2 + t_2^2) \right]. \quad (\text{A1})
\end{aligned}$$

Integrating over \vec{X}_{ν_e} ,

$$\begin{aligned}
\int d\vec{X}_{\nu_e} |I^{\text{normal}}(\delta p)|^2 &= 8 \frac{\pi^{\frac{9}{2}} (\sigma_\mu \sigma_{\nu_e})^3}{(\sigma_\mu + \sigma_{\nu_e})^{\frac{3}{2}}} \exp \left[-\frac{\sigma_\mu + \sigma_{\nu_e}}{(\vec{v}_{\nu_e} - \vec{v}_\mu)^2} (\delta p^0 - \vec{v}_0 \cdot \delta \vec{p})^2 \right] \\
&\times \exp \left[-\frac{\sigma_\mu \sigma_{\nu_e}}{\sigma_\mu + \sigma_{\nu_e}} \delta \vec{p}^2 \right] \int dt_1 dt_2 e^{-\frac{t_1+t_2}{\tau_\mu}} \\
&\times \exp \left[-\frac{(\vec{v}_{\nu_e} - \vec{v}_\mu)^2}{4(\sigma_\mu + \sigma_{\nu_e})} \left\{ t_1 - t_2 - 2i \frac{(\sigma_\mu + \sigma_{\nu_e}) (\delta p^0 - \vec{v}_0 \cdot \delta \vec{p})}{(\vec{v}_{\nu_e} - \vec{v}_\mu)^2} \right\}^2 \right].
\end{aligned} \tag{A2}$$

For the wave packets of

$$\sqrt{\frac{\sigma_\mu + \sigma_{\nu_e}}{(\vec{v}_\mu - \vec{v}_{\nu_e})^2}} \ll \tau_\mu, \tag{A3}$$

and T of

$$\sqrt{\frac{\sigma_\mu + \sigma_{\nu_e}}{(\vec{v}_\mu - \vec{v}_{\nu_e})^2}} \ll T, \tag{A4}$$

we have

$$\begin{aligned}
\int d\vec{X}_{\nu_e} |I^{\text{normal}}(\delta p)|^2 &= 16 \frac{\pi^5 (\sigma_\mu \sigma_{\nu_e})^{\frac{3}{2}}}{(\sigma_\mu + \sigma_{\nu_e}) |\vec{v}_{\nu_e} - \vec{v}_\mu|} \exp \left[-\frac{\sigma_\mu + \sigma_{\nu_e}}{(\vec{v}_{\nu_e} - \vec{v}_\mu)^2} (\delta p^0 - \vec{v}_0 \cdot \delta \vec{p})^2 \right] \\
&\times \exp \left[-\frac{\sigma_\mu \sigma_{\nu_e}}{\sigma_\mu + \sigma_{\nu_e}} \delta \vec{p}^2 \right] \frac{\tau_\mu}{2} \left(1 - e^{-\frac{2T}{\tau_\mu}} \right).
\end{aligned} \tag{A5}$$

For the parameter region outside Eqs. (A3) and (A4), the probability from normal term are computed numerically. The numerical result for μDAR is shown in Fig. (18).

Appendix B: Light-cone singularity

The light-cone singularities from general correlation functions used in this paper are summarized.

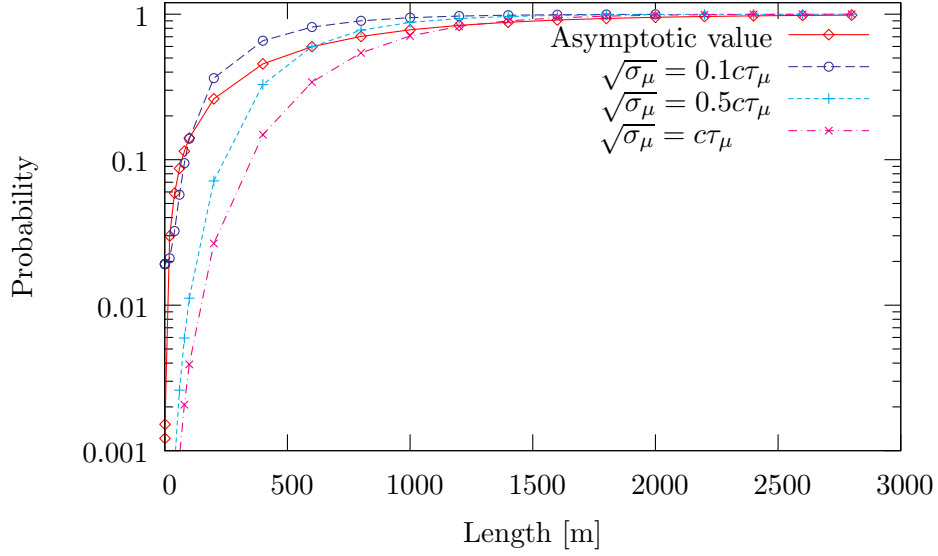


FIG. 18. (Color online) σ_μ dependence of the probability of μ DAR normalized to 1 at $T = \infty$. The probabilities computed with plane waves (asymptotic value) (red), $\sqrt{\sigma_\mu} = 0.1c\tau_\mu$ (deep blue), $\sqrt{\sigma_\mu} = 0.5c\tau_\mu$ (light blue), and $\sqrt{\sigma_\mu} = c\tau_\mu$ are given. We assume $\sigma_\mu \gg \sigma_{\nu_e}$. Deviations from simple exponential decay are significant at $L < c\tau_\mu$.

1. Vacuum expectation value

a. Real mass

The correlation function $D^+(\delta t, \delta \vec{x}; m)$ of a relativistic particle of mass m is given in the form:

$$\begin{aligned}
 D^+(\delta t, \delta \vec{x}; m) &= \frac{1}{i^2(2\pi)^4} \int d^4q \left[\frac{1}{q_0^2 - \vec{q}^2 - m^2 - i\epsilon} - \frac{1}{q_0^2 - \vec{q}^2 - m^2 + i\epsilon} \right] e^{iq \cdot \delta x} \theta(q_0) \\
 &= \frac{\epsilon(\delta t)}{4\pi} \delta(\lambda) - \frac{im}{8\pi\sqrt{\lambda}} \theta(\lambda) \left[N_1(m\sqrt{\lambda}) - i\epsilon(\delta t) J_1(m\sqrt{\lambda}) \right] \\
 &\quad + \theta(-\lambda) \frac{im}{4\pi^2\sqrt{-\lambda}} K_1(m\sqrt{-\lambda}), \tag{B1}
 \end{aligned}$$

where $\epsilon(\delta t) = \pm 1$ is sign function of δt , and N_1 , J_1 , and K_1 are Bessel functions. The integrand vanishes in $q^2 = q_0^2 - \vec{q}^2 < 0$, and $D^+(\delta t, \delta \vec{x}; m)$ decreases exponentially at $\lambda < 0$, oscillates at $\lambda > 0$, and has a singularity at the light cone $\lambda = 0$ of the universal form.

b. Imaginary mass

The correlation function $D^+(\delta t, \delta \vec{x}; im)$ is given in the form:

$$\begin{aligned} D^+(\delta t, \delta \vec{x}; im) &= \frac{1}{i^2(2\pi)^4} \int d^4q \left[\frac{1}{q_0^2 - \vec{q}^2 + m^2 - i\epsilon} - \frac{1}{q_0^2 - \vec{q}^2 + m^2 + i\epsilon} \right] e^{iq \cdot \delta x} \theta(q_0) \\ &= \frac{\epsilon(\delta t)}{4\pi} \delta(\lambda) - \frac{m}{8\pi\sqrt{-\lambda}} \theta(-\lambda) \left[N_1\left(m\sqrt{-\lambda}\right) - i\epsilon(\delta t) J_1\left(m\sqrt{-\lambda}\right) \right] \\ &\quad + \theta(\lambda) K_1\left(m\sqrt{\lambda}\right). \end{aligned} \quad (\text{B2})$$

The integrand vanishes in $q^2 = q_0^2 - \vec{q}^2 > 0$, and $D^+(\delta t, \delta \vec{x}; im)$ decreases exponentially at $\lambda > 0$, oscillates at $\lambda < 0$, and has a singularity at the light cone $\lambda = 0$ of the universal form.

2. Single particle expectation value

The correlation function $D^+(\delta t, \delta \vec{x}; p, m)$ of an external momentum p is

$$D^+(\delta t, \delta \vec{x}; p, m) = \frac{1}{i^2(2\pi)^4} \int d^4q \left[\frac{1}{q_0^2 - \vec{q}^2 - m^2 - i\epsilon} - \frac{1}{q_0^2 - \vec{q}^2 - m^2 + i\epsilon} \right] e^{i(q-p) \cdot \delta x} \theta(q_0), \quad (\text{B3})$$

and is written as

$$D^+(\delta t, \delta \vec{x}; p, m) = e^{-ip \cdot \delta x} D^+(\delta t, \delta \vec{x}, m), \quad p^2 = m_0^2. \quad (\text{B4})$$

Substituting the singularity of Eq. (B1) into Eq. (B4), we have at $\lambda = 0$

$$D^+(\delta t, \delta \vec{x}; p, m) = e^{-ip \cdot \delta x} \frac{\epsilon(\delta t)}{4\pi} \delta(\lambda) = \frac{\epsilon(\delta t)}{4\pi} \delta(\lambda) e^{-i(p_0 - |\vec{p}| \cos \theta) \delta t}, \quad (\text{B5})$$

which oscillates with δt along the light cone. The above singularity comes from an integral over the momentum of $|\vec{q}| \rightarrow \infty$.

Now, this correlation function includes the singularity of the form, $\delta(\lambda)\epsilon(\delta t)$, from $|\vec{q} - \vec{p}| \rightarrow \infty$. We compute it by writing Eq. (B3) in the form

$$D^+(\delta t, \delta \vec{x}; p, m) = D_\infty^+(\delta t, \delta \vec{x}; p, m) + D_{\text{finite}}^+(\delta t, \delta \vec{x}; p, m), \quad (\text{B6})$$

where $D_\infty^+(\delta t, \delta \vec{x}; p, m)$ and $D_{\text{finite}}^+(\delta t, \delta \vec{x}; p, m)$ are the integral over $p_0 \leq q_0$ and $0 \leq q_0 \leq p_0$, respectively. For $\tilde{m}^2 = m_0^2 - m^2 > 0$, we write the former integral with the variable conjugate

to δx , $r = q - p$, and expand the denominators with $2p \cdot r$,

$$\begin{aligned} D_{\infty}^{+}(\delta t, \delta \vec{x}; p, m) &= \frac{1}{i^2(2\pi)^4} \int d^4 r \left[\frac{1}{r^2 + m_0^2 + 2p \cdot r - m^2 - i\epsilon} - \frac{1}{r^2 + m_0^2 + 2p \cdot r - m^2 + i\epsilon} \right] e^{ir \cdot \delta x} \\ &= D_m(\xi) D_{\infty}^{+}(\delta t, \delta \vec{x}; i\tilde{m}), \end{aligned} \quad (\text{B7})$$

$$\tilde{m} = \sqrt{m_0^2 - m^2}, \quad \xi = -2ip \cdot \frac{\partial}{\partial \delta x}, \quad D_m(\xi) = \sum_{l=0} \frac{\xi^l}{l!} \left(\frac{\partial}{\partial \tilde{m}^2} \right)^l,$$

$$\begin{aligned} D_m(\xi) D_{\infty}^{+}(\delta t, \delta \vec{x}; i\tilde{m}) &= \frac{\epsilon(\delta t)}{4\pi} \delta(\lambda) + D_m(\xi) \left[-\frac{\tilde{m}}{8\pi\sqrt{-\lambda}} \theta(-\lambda) \left\{ N_1(\tilde{m}\sqrt{-\lambda}) \right. \right. \\ &\quad \left. \left. - i\epsilon(\delta t) J_1(\tilde{m}\sqrt{-\lambda}) \right\} + \theta(\lambda) \frac{\tilde{m}}{4\pi^2\sqrt{\lambda}} K_1(\tilde{m}\sqrt{\lambda}) \right]. \end{aligned} \quad (\text{B8})$$

$D_{\infty}^{+}(\delta t, \delta \vec{x}; p, m)$ has the light-cone singularity and regular terms. The former is independent of p and m . These expressions are valid as far as the series converges. The condition for the convergence is expressed in Eq. (62) of the text.

The integral over the region $-p_0 \leq r_0 \leq 0$ is written as,

$$D_{\text{finite}}^{+}(\delta t, \delta \vec{x}; p, m) = \frac{1}{i(2\pi)^3} \int \frac{d\vec{q}}{E(\vec{q})} e^{i(q-p) \cdot \delta x} \theta(p_0 - E(\vec{q})). \quad (\text{B9})$$

For $\tilde{m}^2 < 0$, $D^{+}(\delta t, \delta \vec{x}; p, m) = 0$.

a. High spin component

The correlation function $D^{+}(\delta t, \delta \vec{x}; p, m)_{\alpha_1, \alpha_2, \dots}$ of Lorentz indices are

$$\begin{aligned} D^{+}(\delta t, \delta \vec{x}; p, m) &= \frac{1}{i^2(2\pi)^4} \int d^4 q q_{\alpha_1} q_{\alpha_2} \cdots \left[\frac{1}{q^2 + m^2 - i\epsilon} - \frac{1}{q^2 + m^2 + i\epsilon} \right] e^{i(q-p) \cdot \delta x} \theta(q_0) \\ &= \left(p_{\alpha_1} - i \frac{\partial}{\partial \delta x^{\alpha_1}} \right) \left(p_{\alpha_2} - i \frac{\partial}{\partial \delta x^{\alpha_2}} \right) \cdots D^{+}(\delta t, \delta \vec{x}; p, m), \quad \text{for } \tilde{m}^2 \geq 0, \end{aligned} \quad (\text{B10})$$

$$D^{+}(\delta t, \delta \vec{x}; p, m) = 0, \quad \text{for } \tilde{m}^2 \leq 0. \quad (\text{B11})$$

3. Many-particle expectation value

The correlation function $D^{+}(\delta t, \delta \vec{x}; p, m)_{\alpha_1, \alpha_2, \dots}$ of many-body states are expressed with the mass spectrum, $\rho(m^2)$, as

$$\int dm^2 \rho(m^2) D^{+}(\delta t, \delta \vec{x}; p, m), \quad (\text{B12})$$

where

$$\rho(m^2) = \int d(\text{phase space}) \delta \left(m^2 - \left(\sum_l p_l \right)^2 \right). \quad (\text{B13})$$

a. Two-particle: neutrino and electron

$\Delta_{e,\nu_\mu}(\delta x)$ defined by

$$\Delta_{e,\nu_\mu}(\delta x) = \frac{1}{(2\pi)^6} \int_{-\infty}^{\infty} \frac{d\vec{p}_e d\vec{p}_{\nu_\mu}}{E_e E_{\nu_\mu}} (p_\mu \cdot p_{\nu_e}) (p_e \cdot p_{\nu_\mu}) e^{i(p_e + p_{\nu_\mu} - p_\mu) \cdot \delta x}, \quad (\text{B14})$$

is written with $Q = p_e + p_{\nu_\mu}$

$$\begin{aligned} \Delta_{e,\nu_\mu}(\delta x) &= \frac{1}{(2\pi)^6} \int d^4 Q \delta^{(4)}(p_e + p_{\nu_\mu} - Q) \int_{-\infty}^{\infty} \frac{d\vec{p}_e d\vec{p}_{\nu_\mu}}{E_e E_{\nu_\mu}} (p_\mu \cdot p_{\nu_e}) (p_e \cdot p_{\nu_\mu}) e^{i(Q - p_\mu) \cdot \delta x} \\ &= \frac{1}{(2\pi)^6} \int d^4 Q (p_\mu \cdot p_{\nu_e}) \frac{Q^2 - m_e^2}{2} F(Q), \end{aligned} \quad (\text{B15})$$

where

$$\begin{aligned} F(Q) &= \int_{-\infty}^{\infty} \frac{d\vec{p}_e d\vec{p}_{\nu_\mu}}{E_e E_{\nu_\mu}} \delta^{(4)}(p_e + p_{\nu_\mu} - Q) \\ &= 2\pi \left(1 - \frac{m_e^2}{Q^2} \right) \theta(Q_0) \theta(Q^2 - m_e^2). \end{aligned} \quad (\text{B16})$$

Finally, we write the integral with $m^2 = Q^2$

$$\begin{aligned} \Delta_{e,\nu_\mu}(\delta x) &= \frac{1}{(2\pi)^6} \int d^4 Q (p_\mu \cdot p_{\nu_e}) \frac{Q^2 - m_e^2}{2} e^{i(Q - p_\mu) \cdot \delta x} F(Q) \\ &= \frac{p_\mu \cdot p_{\nu_e}}{2(2\pi)^2} \int dm^2 \left(m^2 - 2m_e^2 + \frac{m_e^4}{m^2} \right) iD^+(\delta t, \delta \vec{x}; p_\mu, m) \\ &= i \frac{p_\mu \cdot p_{\nu_e}}{8\pi^2} \int dm^2 \left(m^2 - 2m_e^2 \frac{m_e^4}{m^2} \right) D^+(\delta t, \delta \vec{x}; p_\mu, m). \end{aligned} \quad (\text{B17})$$

b. Two-particle: two neutrinos

Similarly, $\Delta_{\nu_\mu, \nu_e}(\delta x)$ defined by

$$\Delta_{\nu_\mu, \nu_e}(\delta x) = \frac{1}{(2\pi)^6} \int_{-\infty}^{\infty} \frac{d\vec{p}_{\nu_\mu} d\vec{p}_{\nu_e}}{E_{\nu_\mu} E_{\nu_e}} (p_\mu \cdot p_{\nu_e}) (p_e \cdot p_{\nu_\mu}) e^{i(p_{\nu_\mu} + p_{\nu_e} - p_\mu) \cdot \delta x}, \quad (\text{B18})$$

is written with $Q = p_{\nu_\mu} + p_{\nu_e}$

$$\begin{aligned} \Delta_{\nu_\mu, \nu_e}(\delta x) &= \frac{1}{(2\pi)^6} \int d^4 Q \delta^{(4)}(p_{\nu_\mu} + p_{\nu_e} - Q) \int_{-\infty}^{\infty} \frac{d\vec{p}_{\nu_\mu} d\vec{p}_{\nu_e}}{E_{\nu_\mu} E_{\nu_e}} \\ &= \frac{p_\mu^\alpha p_e^\beta}{(2\pi)^6} \int d^4 Q e^{i(Q - p_\mu) \cdot \delta x} F_{\alpha, \beta}(Q), \end{aligned} \quad (\text{B19})$$

where

$$\begin{aligned}
F_{\alpha,\beta}(Q) &= \int_{-\infty}^{\infty} \frac{d\vec{p}_{\nu_\mu} d\vec{p}_{\nu_e}}{E_{\nu_\mu} E_{\nu_e}} \delta^{(4)}(p_{\nu_\mu} + p_{\nu_e} - Q) (p_{\nu_e})_\alpha (p_{\nu_\mu})_\beta \\
&= \frac{\pi}{6} (g_{\alpha,\beta} Q^2 + 2Q_\alpha Q_\beta) \theta(Q_0) \theta(Q^2).
\end{aligned} \tag{B20}$$

Finally, we have the expression using m^2

$$\begin{aligned}
\Delta_{\nu_\mu, \nu_e}(\delta x) &= \frac{1}{12(2\pi)^5} \int dm^2 \theta(m^2) \int d^4 Q \delta(Q^2 - m^2) \theta(Q_0) \theta(Q^2) \\
&\quad \times (Q^2(p_\mu \cdot p_e) + 2(Q \cdot p_\mu)(Q \cdot p_e)) e^{i(Q-p_\mu) \cdot \delta x} \\
&= \frac{i}{12(2\pi)^2} \int dm^2 \left(m^2(p_\mu \cdot p_e) + 2p_\mu \cdot \left(p_\mu - i \frac{\partial}{\partial \delta x} \right) p_e \cdot \left(p_\mu - i \frac{\partial}{\partial \delta x} \right) \right) \\
&\quad \times D^+(\delta t, \delta \vec{x}; p_\mu, m).
\end{aligned} \tag{B21}$$

Appendix C: Universal function $\tilde{g}(\omega, T; \tau_\mu)$

The finite-size corrections depend on the boundary conditions. But the universal function denoted as $\tilde{g}(\omega, T; \tau_\mu)$ determines their behaviors and is summarized here.

The integral over the coordinates x_1, x_2 and \vec{X}_{ν_e} in Eq. (63) is generally written as

$$\begin{aligned}
&\int d\vec{X}_{\nu_e} \int d^4 x_1 d^4 x_2 e^{ip_{\nu_e} \cdot \delta x} f(\delta x) \prod_{i=1,2} w(x_i, X_\mu; \sigma_\mu) w(x_i, X_{\nu_e}; \sigma_{\nu_e}) e^{-\frac{t_1+t_2}{\tau_\mu}} \\
&= \left(\frac{\pi \sigma_\mu \sigma_{\nu_e}}{\sigma_\mu + \sigma_{\nu_e}} \right)^{\frac{3}{2}} \int d\vec{X}_{\nu_e} e^{-\frac{(\vec{X}_\mu - \vec{X}_{\nu_e})^2}{\sigma_\mu + \sigma_{\nu_e}} T} \int dt_1 dt_2 d\delta \vec{x} e^{ip_{\nu_e} \cdot \delta x} e^{-\frac{1}{4\sigma_\mu} (\delta \vec{x} - \vec{v}_\mu \delta t)^2 - \frac{1}{4\sigma_{\nu_e}} (\delta \vec{x} - \vec{v}_{\nu_e} \delta t)^2} \\
&\quad \times e^{-\frac{t_1+t_2}{\tau_\mu}} \exp \left[-\frac{(\vec{v}_\mu - \vec{v}_{\nu_e})^2}{\sigma_\mu + \sigma_{\nu_e}} \left(\frac{t_1+t_2}{2} - \tilde{T}_L \right)^2 \right] f(\delta x), \\
&\tilde{T}_L = \frac{(\vec{v}_\mu - \vec{v}_{\nu_e}) \cdot (\vec{X}_\mu - \vec{X}_{\nu_e})}{(\vec{v}_\mu - \vec{v}_{\nu_e})^2},
\end{aligned} \tag{C1}$$

and using Gaussian approximation for integration in \vec{X}_{ν_e} , we have

$$(\pi^2 \sigma_\mu \sigma_{\nu_e})^{\frac{3}{2}} \int dt_1 dt_2 d\delta \vec{x} e^{ip_{\nu_e} \cdot \delta x} e^{-\frac{1}{4\sigma_\mu} (\delta \vec{x} - \vec{v}_\mu \delta t)^2 - \frac{1}{4\sigma_{\nu_e}} (\delta \vec{x} - \vec{v}_{\nu_e} \delta t)^2} e^{-\frac{t_1+t_2}{2\tau_\mu}} f(\delta x). \tag{C2}$$

For $f(x) = i\frac{\epsilon(\delta t)}{4\pi}\delta(\lambda)$, integral in Eq. (C2) is written as

$$\begin{aligned}
& \int dt_1 dt_2 d\vec{x} e^{ip_{\nu_e} \cdot \delta x} e^{-\frac{1}{4\sigma_\mu}(\delta\vec{x} - \vec{v}_\mu \delta t)^2 - \frac{1}{4\sigma_{\nu_e}}(\delta\vec{x} - \vec{v}_{\nu_e} \delta t)^2} \frac{i}{4\pi} \delta(\lambda) \epsilon(\delta t) e^{-\frac{t_1+t_2}{2\tau_\mu}} \\
&= \int_0^T dt_1 dt_2 e^{-\frac{(\vec{v}_\mu - \vec{v}_{\nu_e})^2 \delta t^2}{4\sigma_\mu}} \int d\vec{r} e^{ip_{\nu_e} \cdot \delta x} e^{-\frac{(\vec{r} - \vec{v}_{\nu_e} \delta t)^2}{4\sigma_{\nu_e}}} \frac{i}{4\pi} \delta(\lambda) \epsilon(\delta t) e^{-\frac{t_1+t_2}{2\tau_\mu}} \\
&\simeq \frac{i}{2} \sigma_{\nu_e} \int_0^T dt_1 dt_2 e^{-\frac{(\vec{v}_\mu - \vec{v}_{\nu_e})^2 \delta t^2}{4\sigma_\mu}} e^{-\frac{(1-|\vec{v}_{\nu_e}|)^2}{4\sigma_{\nu_e}} \delta t^2} \frac{e^{i\omega_{\nu_e} \delta t}}{\delta t} e^{-\frac{t_1+t_2}{2\tau_\mu}}, \tag{C3}
\end{aligned}$$

where $\omega_{\nu_e} = \frac{m_{\nu_e}^2}{2E_{\nu_e}}$, and $\sigma_{\nu_e} |\vec{p}_{\nu_e}| \ll T$ is used. Due to the small mass of neutrino, $e^{-\frac{(1-|\vec{v}_{\nu_e}|)^2}{4\sigma_{\nu_e}}} \approx 1$ but this suppression factor cannot be ignored for massive particles. The case for $\sigma_\mu \rightarrow \infty$ is summarized first. In this limit, the integral over t_1 and t_2 is generally written as $\mathcal{C}g(\omega_\nu, T; \tau_\mu)$ where $g(\omega_\nu, T; \tau_\mu)$ is dimension-less function and \mathcal{C} is constant in ω_ν . Since $g(\omega_\nu, \infty; \tau_\mu)$ is cancelled with the term from J_{regular} in Eq. (61), it is convenient to define $\tilde{g}(\omega_\nu, T; \tau_\mu) = g(\omega_\nu, T; \tau_\mu) - g(\omega_\nu, \infty; \tau_\mu)$. This new universal function $\tilde{g}(\omega_\nu, T; \tau_\mu)$ determines the behavior of the finite-size correction.

1. General form of $\tilde{g}(\omega_\nu, T; \tau_\mu)$

a. Without mixing

We study the universal function without mixing first and have

$$\begin{aligned}
\mathcal{C}g(\omega_\nu, T; \tau_\mu) &= \frac{i}{2} \int_0^T dt_1 dt_2 \frac{e^{i\omega_\nu(t_1-t_2)}}{t_1 - t_2} e^{-\frac{t_1+t_2}{2\tau_\mu}} \\
&= \frac{i}{2} \int_{-T}^0 dt_- \int_{-\frac{1}{2}t_-}^{T+\frac{1}{2}t_-} dt_+ \frac{e^{i\omega_\nu t_-}}{t_-} e^{-\frac{t_+}{\tau_\mu}} + \int_0^T dt_- \int_{\frac{1}{2}t_-}^{T-\frac{1}{2}t_-} dt_+ \frac{e^{i\omega_\nu t_-}}{t_-} e^{-\frac{t_+}{\tau_\mu}} \\
&= -\tau_\mu \int_0^T dt \frac{\sin(\omega_\nu t)}{t} \left(e^{-\frac{t}{2\tau_\mu}} - e^{-\frac{1}{2\tau_\mu}(2T-t)} \right), \tag{C4}
\end{aligned}$$

where $t_+ = \frac{t_1+t_2}{2}$, $t_- = t_1 - t_2$, $\mathcal{C} = \tau_\mu$ and

$$g(\omega_\nu, \infty; \tau_\mu) = -\arctan(2\omega_\nu \tau_\mu). \tag{C5}$$

Then,

$$\tilde{g}(\omega_\nu, T; \tau_\mu) = \arctan(2\omega_\nu \tau_\mu) - \int_0^T dt \frac{\sin(\omega_\nu t)}{t} \left(e^{-\frac{t}{2\tau_\mu}} - e^{-\frac{1}{2\tau_\mu}(2T-t)} \right). \tag{C6}$$

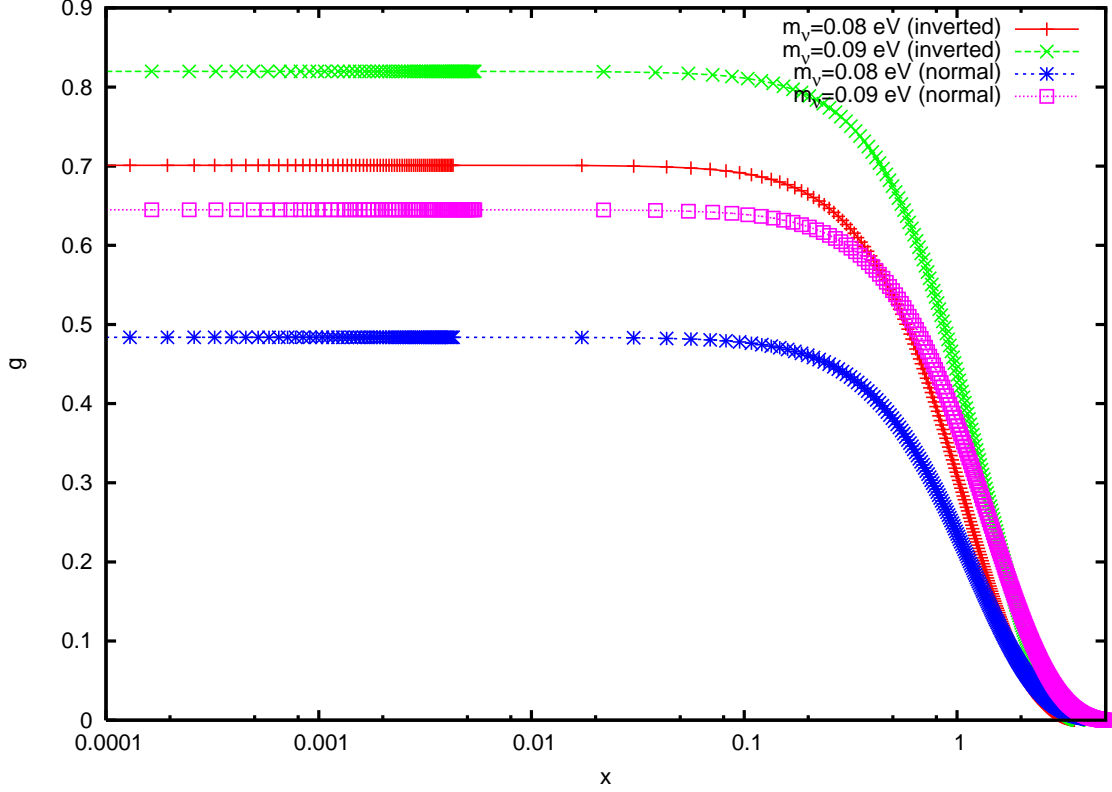


FIG. 19. (Color online) $\tilde{g}_{e,e}(\omega_{\nu_e}, T; \tau_\mu)$ of including flavor mixing, Eq. (C9), is shown. The horizontal axis is $x = \omega_{\nu_h} T$, where $\omega_{\nu_h} = \frac{m_{\nu_h}^2}{2E_{\nu_e}}$, m_{ν_h} is the mass of the heaviest neutrino. Color difference represent differences of mass values of $m_{nu_h} = 0.09$ eV (green: inverted hierarchy, magenta: normal) and $m_{\nu_h} = 0.08$ eV (red: inverted, blue: normal).

b. Mixing case

Originally, the light-cone singularity is computed with mass eigen state. Because flavor states of neutrino are superpositions of mass eigen states, the mixing matrix should be included to the diffraction terms. With mass eigen states of m_i and m_j , we have

$$\begin{aligned} \mathcal{C}g(\omega_i, \omega_j, T; \tau_\mu) = & -\frac{\tau_\mu}{1 + \tau_\mu^2(\omega_i - \omega_j)^2} \int_0^T dt \frac{\sin\left((\omega_i + \omega_j)\frac{t}{2}\right)}{t} \\ & \times \left[e^{-\frac{t}{2\tau_\mu}} \left\{ \cos\left((\omega_i - \omega_j)\frac{t}{2}\right) - \tau_\mu(\omega_i - \omega_j) \sin\left((\omega_i - \omega_j)\frac{t}{2}\right) \right\} \right. \\ & \left. - e^{-\frac{1}{2\tau_\mu}(2T-t)} \left\{ \cos\left((\omega_i - \omega_j)\left(T - \frac{t}{2}\right)\right) - \tau_\mu(\omega_i - \omega_j) \sin\left((\omega_i - \omega_j)\left(T - \frac{t}{2}\right)\right) \right\} \right], \end{aligned} \quad (C7)$$

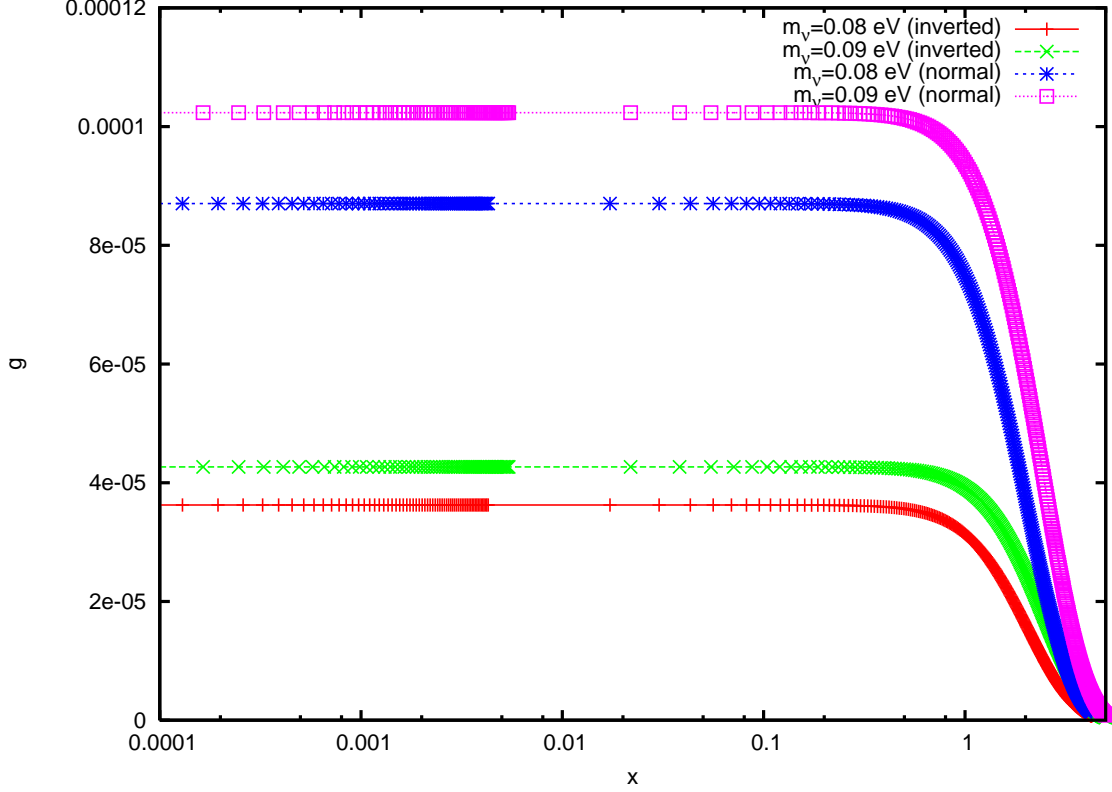


FIG. 20. (Color online) $\tilde{g}_{\mu,e}(\omega_{\nu_e}, T; \tau_\mu)$ of including flavor mixing, Eq. (C9), is shown. The horizontal axis is $x = \omega_{\nu_h} T$, where $\omega_{\nu_h} = \frac{m_{\nu_h}^2}{2E_{\nu_e}}$, m_{ν_h} is the mass of the heaviest neutrino. Color difference represent differences of mass values of $m_{\nu_h} = 0.09$ eV (green: inverted hierarchy, magenta: normal) and $m_{\nu_h} = 0.08$ eV (red: inverted, blue: normal).

and

$$g(\omega_i, \omega_j, \infty; \tau_\mu) = \frac{1}{1 + \tau_\mu^2(\omega_i - \omega_j)^2} \left[-\frac{1}{2}(\arctan(2\omega_i\tau_\mu) + \arctan(2\omega_j\tau_\mu)) \right. \\ \left. + \frac{\tau_\mu(\omega_i - \omega_j)}{4} [-\log(1 + 4\omega_j^2\tau_\mu^2) + \log(1 + 4\omega_i^2\tau_\mu^2)] \right], \quad (C8)$$

where $\mathcal{C} = \tau_\mu$.

Combining the mixing matrix and neutrino mass m_i with the diffraction term, the universal function is written as

$$\tilde{g}_{\alpha,\beta}(\omega_{\nu_\beta}, T; \tau_\mu) = \sum_{i,j} U_{\beta,i} U_{\alpha,i}^* U_{\beta,j}^* U_{\alpha,j} (g(\omega_i, \omega_j, T; \tau_\mu) - g(\omega_i, \omega_j, \infty; \tau_\mu)), \quad (C9)$$

and shown in Figs. 19 and 20. According to those figures, $\tilde{g}_{\alpha,\beta}(\omega_{\nu_e}, T; \tau_\mu)$ is sensitive to the absolute neutrino mass and mass hierarchy and causes observable effects discussed in the text.

2. Large life-time and T

In the case of $\tau \rightarrow \infty$ that is $\Gamma^0 = 0$, the function Eq. (C4) is changed to

$$\mathcal{C}g(\omega, T; \tau_\mu) = Tg(\omega, T) \equiv -T \left(\int_0^{\omega T} \frac{\sin x}{x} - \frac{1 - \cos \omega T}{\omega T} \right), \quad (\text{C10})$$

where $\mathcal{C} = T$ and

$$g(\omega, \infty) = -\frac{\pi}{2}. \quad (\text{C11})$$

Then we have

$$\tilde{g}(\omega, T) = g(\omega, T) - g(\omega, \infty) = \frac{\pi}{2} - \left(\int_0^{\omega T} dx \frac{\sin x}{x} - \frac{1 - \cos \omega T}{\omega T} \right). \quad (\text{C12})$$

This function is suitable for the correction to the process that does not have normal term $T\Gamma^0$ [25].

a. Asymptotic behavior

For $\omega T \gg 1$, the universal function Eq. (C6) behaves as

$$\tilde{g}(\omega, T; \tau) \propto \frac{1}{\omega T}, \quad (\text{C13})$$

and

$$\tilde{g}(\omega, T; \tau) \sim \frac{2}{\omega T}, \quad (\text{C14})$$

at $\omega\tau \approx 1$ or $\tau \rightarrow \infty$. Although $\tilde{g}(\omega, T; \tau)$ is not analytic function, the asymptotic form can be used to estimate the size of finite-size correction.

3. Large mass

In the case of $1/\omega = T_0 \ll T$, especially $T_0 \approx \hbar/p$, it is difficult to separate the normal term and diffraction term in the finite-size correction. Furthermore, the factor $e^{-\frac{(1-|\vec{v}|)^2}{4\sigma}}$ in Eq. (C3) cannot be ignored for massive particles. This factor involves the decoherence condition owing to the finite size of final state at finite distance. Except for the case that the final state is extremely large, the finite-size correction vanishes at $T \sim \sigma$ and the asymptotic value is satisfactory.

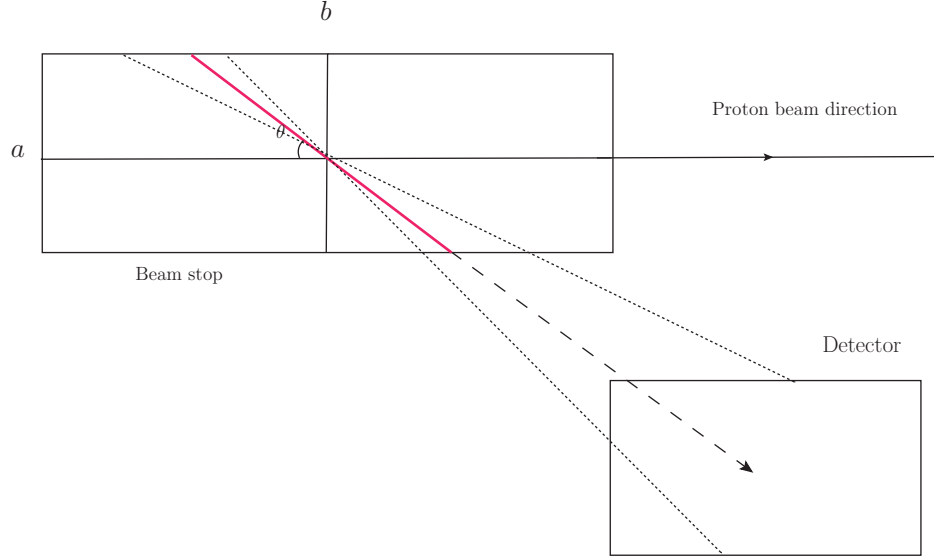


FIG. 21. (Color online) Angle dependence of overlapping region (red line) for μ^+ DAR. It depends on the position and size of detector.

4. Angle dependence of overlapping region T

For μ^+ DAR, the region where parent and daughters overlap is sensitive to the geometry of experiments and diffraction term depends on the angle between a beam axis and detector, even if the decay is spherically symmetric. Following Fig. 21, angle dependence region denoted as T in the text is written as

$$T = \begin{cases} \frac{2a}{\cos(\frac{\pi}{2}-\theta)} & \text{for } 0 \leq \cos \theta < \frac{b}{\sqrt{a^2+b^2}} \\ \frac{2b}{\cos \theta} & \text{for } \frac{b}{\sqrt{a^2+b^2}} \leq \cos \theta, \end{cases} \quad (\text{C15})$$

where θ is the angle between the beam axis and detector, a and b are height and length of the detector, respectively. The probability of the event detected at the detector is averaged over the angle within the detector.

5. σ_μ dependence

a. DAR

For a finite σ_μ , g depends on σ_μ . This case corresponds to μ^- DAR forming a bound state.

$$g(\omega_\nu, T; \tau_\mu) = \int_{-T}^0 dt_- \int_{-\frac{1}{2}t_-}^{T+\frac{1}{2}t_-} dt_+ \frac{|\vec{v}_{\nu_e}| t_- \sin(\omega_{\nu_e} t_-)}{\vec{v}_{\nu_e}^2 t_-^2 + 4|\vec{p}_{\nu_e}|^2 \sigma_{\nu_e}^2} e^{-\frac{(\vec{v}_\mu - \vec{v}_{\nu_e})^2}{\sigma_\mu + \sigma_{\nu_e}} (t_+ - \tilde{T}_L)^2} e^{-\frac{2t_+}{\tau_\mu}} \\ + \int_0^T dt_- \int_{\frac{1}{2}t_-}^{T-\frac{1}{2}t_-} dt_+ \frac{|\vec{v}_{\nu_e}| t_- \sin(\omega_{\nu_e} t_-)}{\vec{v}_{\nu_e}^2 t_-^2 + 4|\vec{p}_{\nu_e}|^2 \sigma_{\nu_e}^2} e^{-\frac{(\vec{v}_\mu - \vec{v}_{\nu_e})^2}{\sigma_\mu + \sigma_{\nu_e}} (t_+ - \tilde{T}_L)^2} e^{-\frac{2t_+}{\tau_\mu}}, \\ t_+ = \frac{t_1 + t_2}{2}, \quad t_- = t_1 - t_2.$$

For μ^+ DAR, μ^+ expands within beam stop and σ_μ is almost the same with T . So σ_μ dependence can be included in T -dependence.

b. DIF

For μ^\pm DIF, σ_μ is determined by parent particles' coherence lengths and estimated as 0.1–1 m [2]. It is good to approximate μ as a plane wave for these values.

-
- [1] K. Ishikawa and Y. Tobita, Prog. Theor. Exp. Phys. **2013**, 073B02 (2013).
 - [2] K. Ishikawa and Y. Tobita, Ann of Phys, **344**, 118 (2014).
 - [3] M. L. Goldberger and K. M. Watson, Phys. Rev. **136**, 1472 (1964).
 - [4] K. Ishikawa and T. Shimomura, Prog. Theor. Phys. **114**, 1201 (2005).
 - [5] J. Beringer, et. al. [Particle Data Group], Phys. Rev. D **86**, 010001 (2012).
 - [6] V. N. Aseev, et. al., Phys. Rev. D **84**, 112003 (2011).
 - [7] E. Komatsu, et. al., Astrophys. J. Suppl., **192**, 18 (2011).
 - [8] G. Hinshaw, et. al., arXiv:1212.5226 [astro-ph.CO].
 - [9] P. A. R. Ade, et. al., arXiv:1303.5076 [astro-ph.CO].
 - [10] K. Ishikawa and Y. Tobita, Prog. Theor. Phys. **122**, 1111 (2009).
 - [11] H. Lehman, K. Symanzik, and W. Zimmermann, Nuovo Cim. **1**, 205 (1955).
 - [12] K. Ishikawa and Y. Tobita, arXiv:1311.6917 [hep-ph].

- [13] R. Jost and H. Lehmann, *Nuovo Cim.* **5**, 1598 (1957).
- [14] F. J. Dyson, *Phys. Rev.* **110**, 1460 (1958).
- [15] K. Ishikawa and Y. Tobita, arXiv:1209.5586 [hep-ph].
- [16] K. Abazajian, M. Acero, S. Agarwalla, A. Aguilar-Arevalo, C. Albright, et al. (2012), arXiv:1204.5379 [hep-ph] and references therein.
- [17] J. Kopp, P. A. N. Machado, M. Maltoni, and T. Schwetz (2013), *JHEP* 1305, 050 (2013).
- [18] A. A. Aguilar-Arevalo et. al., *Phys. Rev. Lett.* 110, 161801 (2013).
- [19] Chen H, et al. (MicroBooNE Collab.) Proposal for a New Experiment Using the Booster and NuMI Neutrino Beamlines. FERMILAB-PROPOSAL-0974. Batavia, Ill.: Fermi Natl. Accel. Lab. (2007); Chen H, et al. (MicroBooNE Collab.) Addendum to Proposal for a New Experiment Using the Booster and NuMI Neutrino Beamlines. Batavia, Ill.: Fermi Natl. Accel. Lab. (2008).
- [20] A. Aguilar, et al., *Phys Rev. D* **64**, 112007 (2001).
- [21] B. Armbruster, et al., *Phys. Rev. D* **65**, 112001 (2002).
- [22] C. Athanassopoulos et al. (LSND Collaboration), *Phys. Rev. C* **58**, 2489 (1998) .
- [23] M. Harada, et al., arXiv:1310.1437 [physics.ins-det].
- [24] D. Adey, et al., arXiv:1308.6822 [physics].
- [25] K. Ishikawa, T. Tajima, and Y. Tobita, in preparation.